Green water availability and water-limited crop yields under a changing climate in Ethiopia

Mosisa Tujuba Wakjira[1], Nadav Peleg[2], Johan Six[3], Peter Molnar[1]

[1]Institute of Environmental Engineering, ETH Zurich, Laura-Hezner-Weg 7, CH-8093 Zürich, Switzerland

5 [2]Institute of Earth Surface Dynamics, University of Lausanne, CH-1015 Lausanne, Switzerland

[3]Institute of Agricultural Science, ETH Zurich, Universitätstrasse 2, CH-8092 Zürich, Switzerland

Correspondence to: Mosisa Tujuba Wakjira (wakjira@ifu.baug.ethz.ch; mosisatujuba@gmail.com)

Abstract. Climate change is expected to influence future agricultural water availability, posing particular challenges in rainfed agricultural systems. This study aims to analyze the climatology of green water availability and water-limited attainable yields

10 (AY) – the maximum crop yield achieved with available green water under optimal soil nutrient and crop management, considering four major cereal crops (teff, maize, sorghum, and wheat) produced in Ethiopia. An agrohydrological modelling framework was developed to simulate climatic-hydrological-crop interactions. The model was applied to a reference (1981-2010) and future periods (2020-2099) under low, intermediate, and high greenhouse gas emission scenarios ~~in order~~ to: (i) evaluate the current green water availability and AY potential; (ii) assess their climate-driven changes; and (iii) analyze the

15 sensitivity of changes in AY to changes in rainfall and atmospheric evaporative demand. With regional variations based on climatic regimes, the main growing season (Meher, May to September) has an average AY of 79 % of a fully irrigated potential yield with an average soil moisture deficit of 29 % of moisture content at full water holding capacity. AY of the short growing season (Belg, February-May) is on average 37 % of the potential yield, with a soil moisture deficit of 56 %. Under the future climate, Meher is expected to experience small changes in the range of ±5 % with dominantly positive trends in the 2030s and

20 decreases in the 2060s and 2080s, mainly driven by changes in the atmospheric evaporative demand due to rising temperatures. The Belg-producing regions are expected to experience increased AY that is dominantly controlled by increases in rainfall. On the other hand, a substantial yield gap is identified between actual and water-limited yields. This points to the need for combining green water management practices with nutrient and tillage management, plant protection, and cultivar improvement to close the yield gaps and ~~to~~ build up the climate resilience of farmers.

25 ## 1. Introduction

Green water, the infiltrated part of rainfall that is stored in the soil root zone and returns to the atmosphere in the form of evapotranspiration (Falkenmark, 2006), is the sole source of moisture in rainfed agriculture (RFA) systems (Rockström, 1999). Green water accounts for an estimated 80 % of the global agricultural evapotranspiration fluxes, and RFA systems produce ~60 % of the global food (Mekonnen and Hoekstra, 2011; Molden et al., 2011; Rockström et al., 2010; Sposito, 2013). The

30 reliance on green water varies across regions, with sub-Saharan Africa (SSA) being particularly dependent on this water

resource, where close to 95 % of croplands are under rainfed agriculture practices (Abrams, 2018; Laderach et al., 2021). Due to the highly dynamic nature of green water availability (GWA), influenced by climatic and biophysical factors that vary in space and time, RFA systems are strongly climate-sensitive under moisture-limited conditions (Kang et al., 2009; Meng et al., 2023; Park et al., 2022). Climate change presents an additional major challenge to the system, undermining crop production with potential consequences of food insecurity, livelihood losses, and economic crises (FAO, 2022).

Previous global-scale assessments have highlighted the challenges posed by climate change on agriculture, both in the past and ~~in~~ the future, leading to regionally varying intensification of agricultural water scarcity and a decrease~~s~~ in crop yields (e.g., Borgomeo et al., 2020; Jägermeyr et al., 2021; Lobell et al., 2011; Rosenzweig et al., 2014). This is particularly evident across the tropics including the highly climate-vulnerable SSA countries (Burke et al., 2009; Kummu et al., 2021; Müller et al., 2011; Rezaei et al., 2023; Rosenzweig et al., 2014; Schlenker and Lobell, 2010). Adaptation actions tailored to specific contexts are now a top priority for mitigating the impacts of climate change-induced water scarcity in rainfed agriculture (RFA) systems, primarily at the national scale through the implementation of National Adaptation Plans (NAP) under the auspices of the United Nations Framework Convention on Climate Change (UNFCCC, 2021) and other programs.

Ethiopia is one of the countries committed to formulating and implementing the NAP, including in agriculture, the sector which the country and its population heavily rely on (FDRE, 2019). In fact, climate adaptation is a much-needed action in Ethiopian smallholder agriculture, of which ~95 % is dependent on GWA, and at the same time it is an indispensable activity supporting the food and income of nearly 80 % of the population. The NAP and its implementations are, in principle, based on analyses of climate change impacts and vulnerability, along with relevant adaptation actions (UNFCCC, 2021; Warren et al., 2018). Previous studies on the crop yield impacts of climate change in Ethiopia have mainly focused on local case studies (e.g., Abera et al., 2018; Araya et al., 2015; Degife et al., 2021; Hadgu et al., 2015; Kassie et al., 2014; Markos et al., 2023; Moges and Gangadhara, 2021), making them patchy and insufficient as a comprehensive guide for the NAP. Here we propose a framework ~~which~~ that allows for a regional comprehensive analysis of agrohydrological responses to climate change across the RFA regions of Ethiopia.

This framework builds on the key factors that influence GWA and their cascading effects on crop yield, to guide appropriate agricultural water management planning, decisions, and actions. Several factors influence GWA. While rainfall amount and distribution fundamentally determine the green water supply, rainfall event characteristics such as intensity, frequency, and duration, combined with surface biophysical conditions (mainly soil, land cover, terrain slope, and roughness), govern the partitioning of rainfall into overland flow and infiltration (Rockström and Gordon, 2001; Schuol et al., 2008). Soil properties (e.g., textural composition, organic matter content, thickness, and salinity) ~~in particular~~ determine the rainfall partitioning to infiltration and runoff, the subsurface flow, green water storage capacity, and plant accessibility, while potential evapotranspiration driven by air temperature, radiation, wind, relative humidity, and vegetation controls the return flow of green water to the atmosphere (Ringersma et al., 2003).

In moisture-limited regions, crop yield is proportional to the magnitude of the evapotranspiration flux, which is constrained by moisture availability (Hatfield and Dold, 2019; Steduto et al., 2012). The maximum yield that can be achieved with the available green water under the best nutrient input and crop management conditions in RFA systems is considered to be the *water-limited attainable yield* (van Ittersum et al., 2013; Lobell et al., 2009). In conditions where water is not a limiting factor, like in RFA systems in humid agroecologies and fully irrigated systems in dry agroecologies, the maximum achievable crop yield is limited by energy, and thus is called *energy-limited yield potential*.

Quantification of the complex interactions between climate, soil, cultivar and crop management is commonly done with mechanistic crop models, for example, APSIM (Holzworth et al., 2014), AquaCrop (Raes et al., 2009; Steduto et al., 2009), CROPSYST (Stöckle et al., 2003), DSSAT (Jones et al., 2003), EPIC (Williams, 1990), and WOFOST (van Diepen et al., 1989), which are used to simulate crop growth and yields at field scale. These models combine hydrological models that simulate hydroclimatic processes to estimate water availability in the root zone, and crop growth models that simulate the crop physiological responses to the agro-environmental and management conditions (Foster and Brozović, 2018; Siad et al., 2019). Model complexity, and associated issues such as high input data and parameter requirements, and computational demand, are major constraints of mechanistic crop models especially when applied in a distributed setting to a large geographic domain, which necessitates a compromise between the level of complexity and the purpose of the modelling (Adam et al., 2011; Ramirez-Villegas et al., 2017).

Here, we employ a simplified agrohydrological modelling framework to assess the impacts of climate change on GWA and the subsequent effects on major cereal crops (teff, maize, sorghum, and wheat) produced in the entire RFA region of Ethiopia. We address three research questions that are relevant for future agricultural water management planning and decision-making in Ethiopia: (i) what is the current green water availability and how will it change under the future climate across the RFA region?; (ii) how will these changes affect water-limited attainable crop yields (AY)?; and (iii) which hydroclimatic factor (rainfall or evapotranspiration) dominantly drives these changes and where? We base our assessment on crop response conditions where all crop growth factors except water are unlimited so that we can capture the effects of climate-driven changes in crop yields in a relative manner. Furthermore, we critically discuss the implications of the changes for water management in the NAP and similar agricultural development initiatives. We also present the workflow of our modeling framework to ensure its robust application in addressing similar or related agrohydrological research questions.

2. Methods

2.1. Study area

The study area covers the entire rainfed arable parts of Ethiopia (hereafter RFA region), as mapped in previous land use analysis (Kassawmar et al., 2018), encompassing an area of about 667,000 km^2 (59 % of the landmass of Ethiopia, see the blue outline in Figure 1a). The climate of the RFA region ranges from humid to semi-arid (Figure 1c) with mean annual potential evapotranspiration ranging from 700 mm in the highland regions to 1800 mm in the western lowland part of the RFA region.

95 The mean annual rainfall of the RFA region ranges from 270 mm in the eastern part to 2100 mm in the western and southwestern parts (Figure 1b). The rainfall has unimodal patterns in the central, western, northern, and northeastern parts with the highest rainfall in July/August depending on the location (Segele and Lamb, 2005; Wakjira et al., 2021). This rainy season typically spans from May to September, coinciding with the main growing season, locally known as 'Meher', during which approximately 88 % of the total annual crop harvest occurs (CSA, 2007). The southern and eastern parts of the RFA region on

100 the other hand, largely experience a bimodal pattern with two rainy seasons in spring and autumn. The spring (February-May) rainy period is considered the second and shorter growing season, locally known as 'Belg', in the southern and southeastern part of the RFA region. Cereals account for about 80 % of the crops produced, with teff, maize, sorghum, wheat, and barley being the top varieties, also serving as the main staple food crops in the country (CSA, 2007, 2010).
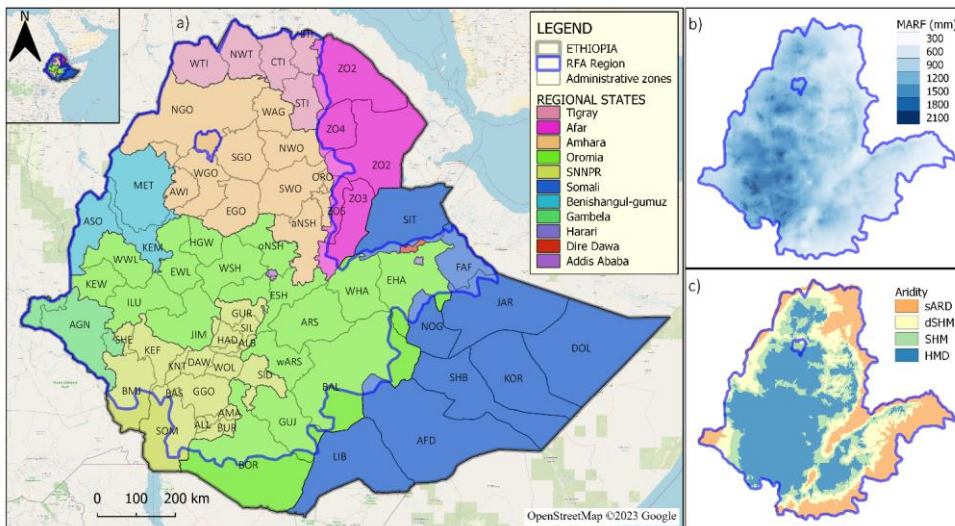
105 **Figure 1: (a) Map of Ethiopia, the spatial extent of the rainfed agricultural region (blue outline, Kassawmar et al., 2018), administrative zones (designated by short names) in the nine regional states. The complete list of the zones with full names is given in Table S1. (b) Mean annual rainfall (MARF) of the RFA area for the period 1981-2010, based on CHIRPS. (c) Climatic regimes (aridity) of the RFA area (classification based on Spinoni et al., (2015)). sARD: semi-arid, dSHM: dry sub-humid, SHM: sub-humid, HMD: humid**

110 **2.2. Data**

Daily rainfall data for the reference period (1981-2010) was obtained from the Climate Hazards Infrared Precipitation with Station (CHIRPS) dataset (Funk et al., 2015), which is available at 0.05° x 0.05° spatial resolution. Maximum and minimum

daily 2-m air temperature data consists of the bias-corrected and downscaled ERA5-Land (BCE5) dataset (Wakjira et al., 2022, 2023), which is also available at 0.05° x 0.05° spatial resolution. Other climate variables (solar radiation, wind speed, and dew point temperature) were retrieved from ERA5-Land (Muñoz-Sabater et al., 2021) and disaggregated to a resolution of 0.05° x 0.05° using a bilinear interpolation method.

Future climate data were derived by downscaling multiple Global Circulation Model (GCM) projections, i.e., 26 for precipitation and solar radiation and 21 for maximum and minimum daily temperatures (listed in Table S2), from their native coarse resolution to 0.05° x 0.05° grid resolution using change factor (delta) approach (e.g., Anandhi et al., 2011; Teutschbein and Seibert, 2012). The future climate scenarios include three Shared Socioeconomic Pathways SSPs (Meinshausen et al., 2020; O'Neill et al., 2016), namely the SSP1-2.6 (low greenhouse gas emission), SSP2-4.5 (intermediate emission) and SSP5-8.5 (high emission).

Gridded soil texture and organic carbon content data were retrieved from SoilGrids (Poggio et al., 2021). Although the SoilGrids soil data is available at 250 m grid resolution, we upscaled the data to 0.05° (~5 km) to harmonize the spatial resolution with that of the climate datasets. Curve number (CN) values for agricultural land use were obtained from the USDA (1985) lookup table according to the hydrologic soil group dataset developed by Ross et al. (2018).

Independent soil moisture (SM), actual evapotranspiration (ETa), surface runoff, and crop ~~production~~ data~~sets~~ were utilized to evaluate the agrohydrological model simulations. Four satellite and model-based global SM datasets, ESA CCI (Dorigo et al., 2017), GLDAS 2.1 (Rui and Beaudoing, 2020), LPMR-TMI (Teng and Parinussa, 2021), and SGD-SM (Zhang et al., 2022), were considered in the evaluation. ETa ~~datasets~~ estimates were retrieved from five products – SSEBop (Senay et al., 2020), PML-v2 (Zhang et al., 2019), MOD16A2 (Mu et al., 2019), GLDAS 2.1 (Rui and Beaudoing, 2020), and TerraClimate (Abatzoglou et al., 2017), covering the period 2003-2010. Surface runoff data were collected from published runoff plot measurements at ~~17~~ 20 locations (Table S3) across the RFA region of Ethiopia. Regarding the crop data, paired water-limited (Yw) and potential yields (Yp) data were collected from published case studies that are based on field trials and calibrated crop model simulation experiments at 26 locations, and from the Global Yield Gap Atlas, GYGA (Global Yield Gap Atlas, 2024), 19 additional locations across the study area (refer Table S4 for more details). In addition to the yield data, total cereal production (TCP), consisting of the sum of all cereals (maize, teff, sorghum, wheat, barley, millet, oat, and rice) produced in Ethiopia, which was derived from the annual Agricultural Sample Survey (AgSS) reports (e.g., CSA, 2010) gridded by Wakjira et al. (2021) for the period 1995-2010, was also utilized in the evaluation.

2.3. Agrohydrological modelling

The agrohydrological modelling framework (Figure 2) that interlinks climate-hydrological-crop (CHC) interactions was developed to simulate the effects of climate change on green water fluxes, and its cascading influences on crop yield. The CHC model consists of three modules for climate, hydrology, and crops.
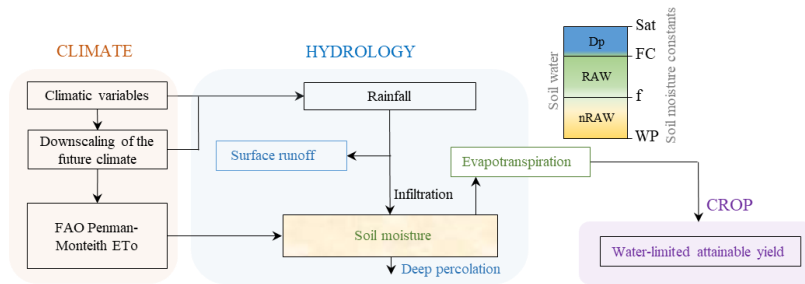
145 **Figure 2: The CHC model used for the assessment of climate-driven changes in green water availability and water-limited attainable yields. Dp = deep percolation, RAW = readily available water, nRAW = non-readily available water, FC = field capacity, WP = wilting point, f = critical moisture depletion factor.**

2.3.1. Climate module

The climate module uses climatic variables to compute the daily reference evapotranspiration ETo [mm d⁻¹] using the FAO
150   Penman-Monteith equation considering a hypothetical reference grass (Allen et al., 1998):

$$\text{ETo} = \frac{0.408\Delta(R_n-G)+\gamma\frac{900}{T+273}u_2(e_s-e_a)}{\Delta+\gamma(1+0.34u_2)}, \tag{1}$$

where R_n [MJ m⁻²] is net radiation at the crop surface, G [MJ m⁻²] is soil heat flux, T [°C] is 2-m mean daily air temperature, u_2 [m s⁻¹] is 2-m daily wind speed, $e_s - e_a$ [kPa] is the saturation vapor pressure deficit, Δ [kPa °C⁻¹] is the slope of the vapor pressure curve, and γ [kPa °C⁻¹] is the psychometric constant.

2.3.2. Hydrology module

155   The hydrology module simulates the dynamic soil water balance without lateral surface and subsurface routing. A conceptual (bucket) water balance model is applied to the soil hydrological fluxes – surface runoff Q [mm], actual evapotranspiration ETa [mm], deep percolation Dp [mm], and changes in soil moisture ΔSM [mm] from rainfall input P [mm] at daily time step t:

$$\Delta SM_t = P_t - Q_t - ETa_t - Dp_t. \tag{2}$$

Surface runoff is simulated according to the US Soil Conservation Service (SCS) curve number method (USDA, 1985).

$$Q_t = \begin{cases} \frac{(P_t-I_{a,t})^2}{(P_t-I_{a,t})+S_{20,t}}, & \text{if } P_t > I_a \\ 0 & , \text{otherwise} \end{cases}. \tag{3}$$

where I_a [mm] is an initial abstraction S [mm] is the maximum surface retention after runoff begins. We chose the SCS curve number method because it provides a reliable estimate of surface runoff with reduced number of model parameters. This method accounts for soil hydrologic properties, land use, and antecedent soil moisture conditions (AMC) to partition rainfall into infiltration and surface runoff. Consequently, the soil water balance components of widely applied crop models such as DSSAT (Jones et al., 2003), AquaCrop (Hsiao et al., 2009; Raes et al., 2009; Steduto et al., 2009), APSIM (Holzworth et al., 2014), CROPSYST (Stöckle et al., 2003), EPIC (Williams, 1990), and SWAT+ (Bieger et al., 2017; Čerkasova et al., 2023), among others are either built entirely built on the SCS curve number method, or provide it as a simpler alternative to infiltration-based models.

Formatted: Font: Italic
Formatted: Font: Italic, Subscript

In the original SCS curve number model, the initial abstraction ratio I_a [mm] of 20 % was assumed so that I_a to beis 20 % of S (indicated by the subscript in Eq. (3)). However, recent insights led to an update in this the abstraction ratio value to 5 %, which yielded higher runoff prediction performance of the SCS model. A proposed conversion function from S_{20} to S_{05} is expressed by Hawkins et al. (2020):

$$S_{05} = 1.42 S_{20}. \tag{4}$$

S is determined by the land surface conditions including soil characteristics as represented by the hydrologic soil group, land use land cover (in our case agricultural land), and antecedent soil moisture, all of which are parameterized as a dimensionless CN value. We estimated S using Eq. (5).

$$S_{20} = 254 \left(\frac{100}{CN} - 1 \right). \tag{5}$$

CN is updated daily for antecedent moisture conditions (AMC), which are often categorized as *dry*, *normal*, and *wet*. The CN values obtained from the USDA lookup table correspond to the *normal* AMC condition. Accordingly, we estimated the CN values for the *dry* and *wet* AMC following Raes et al. (2022) and Smedema and Rycroft (1983):

$$CN_{dry} = 16.91 + 1.348 CN - 0.01379 (CN)^2 + 0.0001172 (CN)^3,$$
$$CN_{wet} = 2.5838 + 1.944 CN - 0.014216 (CN)^2 + 0.000045829 (CN)^3. \tag{6}$$

We then adjusted CN at every time step by linearly interpolating between CN and CN_{dry} or CN_{wet} depending on the soil moisture condition, assuming the soil moisture content corresponds to θ_{WP} for CN_{dry}, $\theta_{0.5(\theta_{FC}+\theta_{WP})}$ for CN, and θ_{FC} for CN_{wet}. Note that θ_{FC} [m³ m⁻³] and θ_{WP} [m³ m⁻³] are volumetric moisture contents at field capacity and wilting point and they were estimated using the widely used pedotransfer function developed by Saxton and Rawls (2006).

Applying the conversion from Eq. (4) for S_{05} and then expressing I_a in terms of S_{20} in Eq. (3), the expression for Q can be rewritten as:

$$Q_t = \begin{cases} \dfrac{(P_t - 0.071S_{20,t})^2}{(P_t + 1.349S_{20,t})} & \text{, if } P_t > 0.071S_{20} \\ 0 & \text{otherwise} \end{cases} \quad . \tag{7}$$

The rainfall that is in excess of Q (Eq. (7)) infiltrates into the soil and refills the available soil storage V_t [mm] = $1000Z(\theta_{sat} - \theta_{t-1})$, where θ_{sat} [m^3 m^{-3}] and θ_{t-1} [m^3 m^{-3}] are volumetric soil moisture content at saturation and on the previous day (respectively), and Z [m] is the soil depth. We considered that the top 60 cm homogeneous soil layer contains the majority of the root biomass (e.g., Fan et al., 2016; Mthandi et al., 2013), and hence this is the agrohydrological active soil depth Z for the major crops. ETa is determined by moisture availability (green water) relative to the readily available water, RAW [mm] = $1000Zf(\theta_{FC} - \theta_{WP})$, where f [-] is a critical depletion fraction that represents the soil moisture level below which plants experience moisture stress. For all four cereal crops studied, the value of f was set to 0.55 following Allen et al. (1998). ETa was computed as $ETa_t = K_{s,t}ET_{o,t}$, where Ks [-] is the soil moisture stress coefficient (Allen et al., 1998):

$$K_{s,t} = \begin{cases} \dfrac{SM_t}{RAW} & \text{if } SM_t < RAW \\ 1 & \text{if } SM_t > RAW \end{cases} \quad . \tag{8}$$

If the soil is saturated, the infiltrated water which ~~is in excess of~~exceeds the soil field capacity percolates into deeper soil layers at the rate $Dp_t = 1000Z(\theta_t - \theta_{FC})$.

2.3.3. Crop module

The crop module simulates water-limited attainable yield (AY) based on the FAO water production function (Doorenbos and Kassam, 1979). The FAO water production function is a well-established relationship between climate and crop yield, explaining relative yield as a function of the evapotranspiration ratio, i.e., the ratio of actual to potential evapotranspiration on a seasonal scale. It is widely applied to assess the effects of water scarcity and climate change impacts on crop yields to inform agricultural water management planning and decision-making (e.g., Fischer et al., 2021; Foster and Brozović, 2018; Geerts and Raes, 2009; He et al., 2022; Sapino et al., 2022; Smilovic et al., 2016).~~;~~ The function assumes ~~which establishes~~ a linear relationship between relative crop yield losses and seasonal evaporative stress (deficits in crop water use) under water-limited climatic conditions:

$$1 - \frac{Y_w}{Y_p} = K_y\left(1 - \frac{ETa}{ETo}\right), \tag{9}$$

where Y_w [ton ha^{-1}] and Y_p [ton ha^{-1}] are water-limited and energy-limited potential yields (respectively), and K_y [-] is the yield response factor that accounts for the complex crop characteristics that determine the crop water use. We redefined for AY, the ratio of water-limited yield Y_w, and potential yield Y_p as a function of evaporative stress index $ESI = 1 - ETa/ETo$:

$$AY = 100(1 - K_y ESI).\qquad(10)$$

205 The recommended K_y values were set to 1.25 for maize, 0.9 for sorghum, and 1.15 for wheat, obtained from the FAO irrigation and drainage paper 66 (Steduto et al., 2012), and to 1.04 for teff (Araya et al., 2011).

2.3.4. Model evaluation

The CHC modelling framework was not explicitely calibrated, meaning all parameters were taken from literature and global dataset., however the results were validated with independent datasets. Due to the limited availability of observed data we
210 could not conduct a formal validation of the model., however However we compared the simulated values of the against the two most important observed agrohydrological variables Q, SM, and ETa, at annual scaleas well as water-limited attainable yield AY with independent data. In our comparisons, we focused on the differences and correlations between the simulated and independent values using the root mean squared difference (RMSD) and the Pearson correlation coefficient (ρ).

The simulated mean annual Q was compared to published mean annual runoff observations from 17 20 sites within the RFA
215 region (Table S3). We used the Nash-Sutcliffe Efficiency (NSE, Nash and Sutcliffe, 1970) and coefficient of determination R^2 to quantify the prediction skill. Similarly, wWe compared the simulated annual cycles and seasonality interannual variabilities of the CHC-simulated SM and ETa with five those of independent satellite- and model-based ETa products (hereafter referred to as global datasets) for the period 2003-2010, across the four climatic regimes – semi-arid, dry sub-humid, sub-humid and humid. For AY, we compared the simulated AY with the ratio of Yw to Yp estimates obtained from published field trials,
220 calibrated crop model simulations, and the GYGA database at a total of 45 locations across the RFA region (Table S4). FinallyAdditionally, we examined how temporal variations in AY explain variabilities in seasonal crop production. For this, we correlated AY and total cereal production (TCP) at each computation grid during the period 1995-2010.

2.4. Assessment of Green water availability and its yield potential

We evaluated the climatology of GWA and AY during the two growing seasons, Meher (May to September) and Belg
225 (February to May) from the simulations for the reference period 1981-2010. We used soil moisture deficit (SMD) as a metric to evaluate GWA:

$$SMD = 100\left(1 - \frac{\theta_{clim}}{\theta_{FC}}\right),\qquad(11)$$

where θ_{clim} [m^3 m^{-3}] is the climatological mean seasonal soil moisture. SMD [%] is a dimensionless metric ranging from 0 (no moisture deficit) to 100% (maximum moisture deficit). The yield metric, AY [%], which was determined using Eq. (10(10) is also a relative quantity that explains the percentage of the energy-limited potential yield that can be viably attained under the
230 actual water-limited conditions when all other agro-environmental factors such as nutrients are not limiting the yield, thus its values range from 0 (no yield) to 100% (non-water-limited potential yield). AY is nonlinearly related to SMD, decreasing with

an increasing moisture deficit (Figure 3). This nonlinearity results from the combined effects of climatic and soil characteristics. Figure 3 also shows that attainable yield diminishes as the soil moisture deficit reaches its maximum, which is about 70% of the soil moisture at field capacity.

235
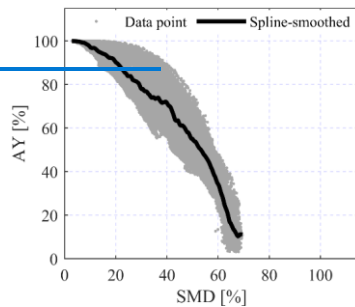
Figure 3: The relationship between AY and SMD in the RFA region of Ethiopia. Each data point represents a single grid cell in the RFA domain considering both Meher and Belg growing seasons.

Commented [MW1]: Moved to the supplementary material

2.5. Future changes and climate sensitivity analysis

We applied the modelling framework to quantify changes in GWA and its implications for AY under climate change. We investigated the changes for three future periods: 2020-2049 (2030s), 2045-2074 (2060s), and 2070-2099 (2080s), under SSP1-2.6 (low), SSP2-4.5 (intermediate), and SSP5-8.5 (high) greenhouse gas emission scenarios. The impact assessments presented here are based on the median of downscaled multiple GCM projections of future changes in rainfall, air temperature, and solar radiation. Other climatic variables were assumed to remain unchanged (Peleg et al., 2019). The impact analyses compare SMD and AY during the three future periods with the reference period (1981-2010) for the two growing seasons, Meher and Belg, and the four major crops grown in Ethiopia (teff, maize, sorghum, and wheat).

We also examined the sensitivity of AY to changes in rainfall (green water supply) and atmospheric evaporative demand (AED) as represented by ETo. We determined the rainfall- and AED-sensitivity metrics, $\beta_{RF} = \frac{\%\Delta AY_{(RF)}}{\%\Delta RF}$ [-] and $\beta_{ED} = \frac{\%\Delta AY_{(ED)}}{\%\Delta ETo}$ [-], as the ratio of percent change in AY and percent change in rainfall or ETo based on the one-at-a-time analysis approach (Hamby, 1994), where the CHC modelling framework was forced by the future RF and ETo (computed considering the future temperature and radiation) for all the three emission scenarios and three future periods. We determined the relative influences of the future changes in rainfall and AED on AY using the sensitivity ratio $\beta_{ratio} = \frac{\beta_{RF}}{\beta_{ED}}$. Values of β_{ratio} [-] range from zero to infinity with values less than one indicating temperature sensitivity dominates and values greater than one indicating AED sensitivity dominates. This assumes that changes in rainfall and ETo are independent, which was confirmed

10

by the low dependency ($R^2 = 0.098$) between rainfall and *ETo* computed for the period 2020-2099 for the three SSPs at every grid point.

3. Results

3.1. Evaluation of the CHC model

We first evaluate the simulated runoff (*Q*), Soil moisture (SM), actual evapotranspiration (ETa), and water-limited attainable yield (AY) against other independent data. The comparison of simulated and observed mean annual *Q* (~~Figure 4~~Figure 4a) at the ~~17~~20 field locations demonstrates a ~~good~~ solid performance (~~ρ~~R^2 = ~~0.80~~0.91 and ~~NSE~~ RMSD = ~~0.53~~52mm) of the hydrological module in estimating the annual surface runoff from croplands. It is important to note that this comparison involves a point-to-grid value, and a perfect match cannot be expected due to this scale difference. The model underestimates the simulated *Q* at the two most humid locations.

The comparison for SM is illustrated in the Figure 4b. The scatter plot of the area-averaged CHC-simulated annual SM (2003-2010) versus the median of that of the global SM datasets demonstrates that the simulated SM closely follows the interannual variabilities in the median of the global datasets, with Pearson's ρ ranging from 0.69 in humid climate to 0.92 in semi-arid climate. Likewise, the annual cycles of the simulated and global SM datasets are also highly comparable, as shown in Figure S1 of the supplementary materials. However, the simulated SM estimates are (systematically) lower than those from the global SM datasets in all climatic regimes (see also Figure S3a and b). These differences decrease from semi-arid (RMSD = 0.075 m^3m^{-3}) to humid areas (RMSD = 0.041 m^3m^{-3}) as shown in Figure 4b. In semi-arid and dry sub-humid areas, these discrepancies can be partly attributed to the fact that satellite-based global SM datasets are informed by vegetation conditions in one way or another (e.g., Dorigo et al., 2017; Rodell et al., 2004; Teng and Parinussa, 2021), which carry soil moisture signatures from deeper soil layers compared to the top 60cm layer considered in this study. But in general, the differences observed in the present analysis is consistent with findings from a previous study by ~~(~~Jimma et al., (2023), which revealed that the global satellite-based soil moisture products (FLDAS, ERA5-Land, ESA CCI, and GLDAS2) significantly overestimate soil moisture over Ethiopia. Similarly, ~~(~~Teferi et al., (2023) also reported that soil moisture estimates derived from two satellite products – Advanced Scatterometer (ASCAT) and Soil Moisture Active Passive (SMAP), overestimate the insitu-measured soil moisture at a monitoring site in the Upper Blue Nile.

~~The comparison for ETa was made for six arbitrarily defined sub-regions of the RFA region as shown in the inset in Figure 4b.~~ The simulated ~~mean~~ annual ETa ~~aligns~~ correlates well with the ~~average~~ median estimates ~~(hereafter, observed) from five independent~~ of the global ETa datasets in all climatic regimes with Pearson's ρ ranging from 0.80 in sub-humid to 0.93 in humid regions (~~Figure 4c~~$R^2 = 0.82$)~~.~~. The annual cycles of the simulated ETa also closely match those of the global ETa datasets (Figure S2). However, during the dry months (December to February), the simulated ETa is lower compared to the global ETa across all climatic regimes. From the scatter plot presented in Figure 4c (see also the spatial patterns in Figure S3c and d), it is evident that the differernces are more pronounced in semi-arid (RMSD = 61mm) and dry sub-humid (31mm)

climates. Like in the case of SM, this can be attributed to the absence of vegetation representation in the CHC modelling framework, unlike in the global ETa datasets considered.~~particularly in the north, northeast, and west sub-regions. Poorest fit is observed in the central sub-region where the model predicts higher ETa than observed, followed by the east sub-region where the simulated ETa is lower than observed. However, the simulated ETa estimates well the monthly cycles (Fig. S1) and~~

290   ~~annual ETa (Fig. S2).~~

The comparisons of the simulated AY (at 45 locations) with three categories of the independent AY estimates are shown in Figure 4d. The green category (scatters) represents the simulated AY versus the corresponding independent AY estimates from field trials and calibrated crop modelling experiments at 20 locations in different years within the reference period (1981-2010) for various crops. These exhibited a good correlation ($\rho = 0.79$) and the smallest difference (RMSD = 7.1 %) compared to the

295   other categories. The blue category represents the simulated AY versus AY estimates from field trials at 6 locations, conducted outside the reference period in later years (post-2010), which we plotted against the average simuated AY over the later years of the reference period (2007-2010). This category also showed a similar correlation to the green category but with higher differences (RMSD = 9.4 %). The orange category, represneting the simulated versus GYGA-derived AY at 19 locations, showed a weaker correlation ($\rho = 0.39$) and the highest difference (RMSD = 14.3 %). Note that these independent data (both

300   from field trials and model simulations) have their own uncertainties. For example, most of the field trials from which the paired Yw and Yp were derived were conducted to evaluate crop yields under supplementary irrigation, not explicitly to determine Yw and Yp. Therefore, the AY derived from these field trials are only estimates. Nevertheless, on average, the CHC-simulated AY is still highly comparable to the independent AY data. The average simulated AY across the 45 locations is 84.2 %, which is slightly lower than the average AY estimate from the independent data, which stands at 86.2 %.
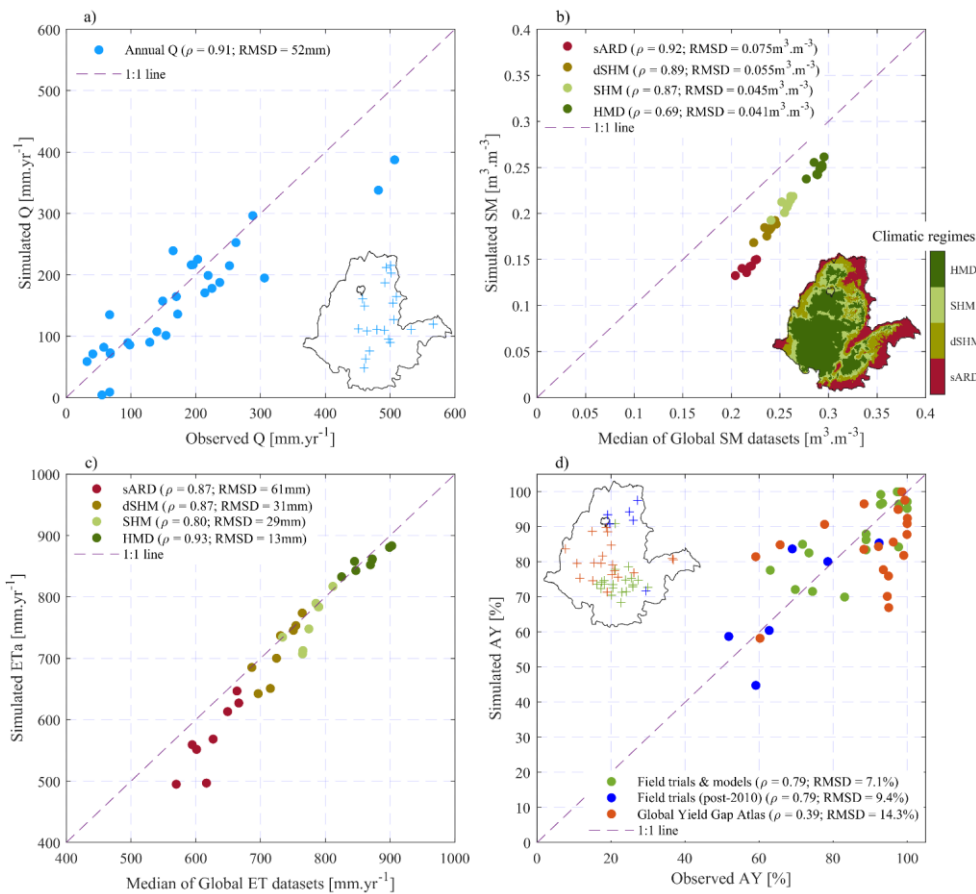
305

Figure 3: Scatter plots of: a) Simulated versus observed yearly or mean annual runoff (Q), measured over varying years at 20 locations (shown on the inset map), collected from published studies across the RFA region (Table S3). This is a grid-to-point comparison. b) Simulated versus median of four satellite- and model-based annual (2003-2010) soil moisture (SM) products (Sect. 2.2) spatially averaged over the four climatic regimes – semi-arid (sARD), dry sub-humid (dSHM), sub-humid (SHM), and humid

310

(HMD) -- shown by the inset map (from Figure 1). Each circle represents area-averaged (over each climatic regime) SM for each year (2003-2010) and the colors indicate the climatic regimes. c) The same as in (b) but for actual evapotranspiration (ETa) considering the median of the five global datasets. d) Simulated water-limited attainable yield (AY) and the observed ratio of water-

limited (rainfed) (Yw) to fully irrigated (Yp) collected published field trials and crop modelling experiments at 29 locations across the RFA region indicated by on the inset map.

315

We also evaluated the simulations of *AY* [%] in terms of their correlation to variations in detrended total cereal production, *TCP* [ton y^{-1}] as depicted in Figure 4. The rationale here is that in some regions TCP will follow the climate-driven attainable yield (high correlation), while in others the non-climatic factors, including nutrient input, improved cultivars, and pest and weed management, will play a role (low or negative correlation). Because TCP in the RFA region of Ethiopia exhibited an
320   average increase of 0.36 ton ha^{-1} y^{-1} during the studied period (1995-2010), despite an almost constant AY, we conducted the correlation analysis on detrended TCP, thereby removing some of the effects of the non-climatic component of the variabilities in TCP (Kukal and Irmak, 2018; Mohammadi et al., 2023; Wakjira et al., 2021). The correlation analysis between detrended TCP and AY anomaly reveals mostly positive correlations (median Pearson's correlation coefficient, $\rho = 0.37$), particularly in the primary Meher-producing northern half of the RFA region (Figure 4Figure 4c).

325   Some areas, primarily in the humid and sub-humid regions of the southern and southwestern parts, and to a lesser extent in the western and southeastern parts of the RFA region, exhibited negative correlations between TCP and AY. This can be attributed to climatic regimes, land use, and socioeconomic practices. Two main factors may govern the AY-TCP correlation with climate. In less water-limited humid areas like the southwestern part, the linear relationship assumed in the crop yield response to water availability (Eq.(9)(9)) does not hold, as AY is weakly dependent on rainfall. Additionally, in these humid climates
330   and areas with poor soil drainage (e.g., areas marked as E1 in Figure 4Figure 4c), crop yield can be adversely affected by saturated soil conditions, leading to waterlogging problems. Concerning land use and socioeconomic practices, the majority of areas with evident negative correlation are forest and/or agroforestry ecoregions (see E2 and E3 in Figure 4Figure 4c) (Kassawmar et al., 2018), while other areas are agropastoral (E4) where seasonal crop production is an optional practice. Thus, interannual variabilities in TCP depend largely on how much farmers opt for cereal production in a given production year.
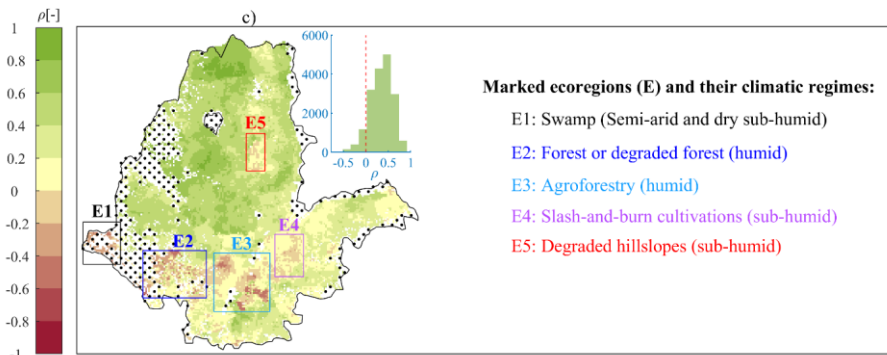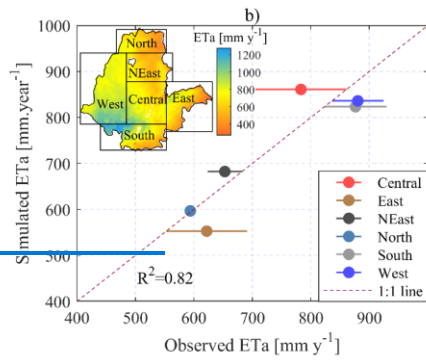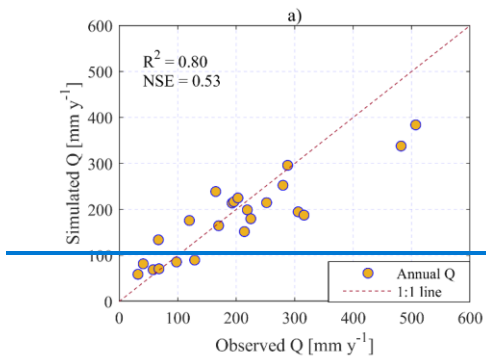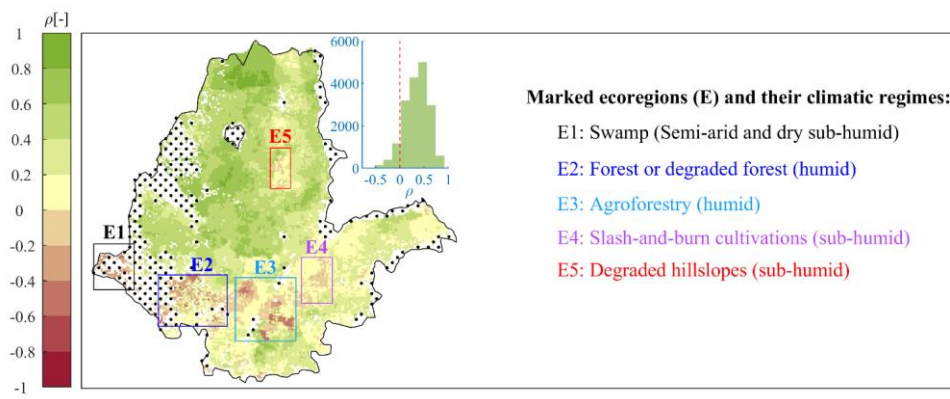
Figure 4: ~~Comparison of: a) Simulated and observed yearly or mean annual runoff (Q), measured over varying years at 17 locations, collected from published studies across the RFA region (Table S3). This is a grid-to-point comparison. b) Simulated and satellite- and model-based mean annual ETa (2003-2010) from five data products (Sect. 2.2) spatially averaged over six arbitrarily defined sub-regions shown on the inset map. The error bars represent the variability (deviation from the median value) of ETa among the five products. c)~~ Map of Pearson's correlation coefficient (ρ) of detrended total cereal production (TCP) and AY for the period 1995-2010. TCP represents the sum of all cereals produced during the Meher growing season with average values ranging from 28 tons to 24,000 tons across the RFA region. The dots show uncultivated areas based on cropland cover fraction data from Copernicus Land Services (Buchhorn et al., 2020). The inset histogram shows the distribution of ρ. The rectangular marks (E1-E5) show ecoregions where the correlations are weak or negative.

3.2. Green water availability and attainable crop yields

The reference climatology of growing season GWA and water-limited yield across the RFA region based on the computed SMD and AY values, is presented in ~~Figure 5~~ Figure 5, considering the reference alfalfa ~~as a reference crop~~grass (Ky = 1.1, ~~(~~Allen et al., 1998~~)~~). During the Meher growing season, the southern and southwestern humid regions of the RFA exhibit low soil moisture deficit, with values less than 10 % of θ_{FC} (see ~~Figure 5~~ Figure 5a). Moving from the southwestern areas, the Meher SMD gradually increases in the northern and northeastern directions. In the peripheral semi-arid regions in the northeast, east, and southeast, the deficit reaches as high as 60-70 %. Notably, areas with SMD values below 20 % largely have AY>90 %. In other words, the water-limited yield gap of less than 10 % of the potential yield achievable under unstressed moisture conditions (equivalent to a fully irrigated system) can be attained in the south-central, southwestern, and eastern highland parts

of the RFA region (Figure 5Figure 5b). As expected, low AY (mostly less than 40 %) is evident in the southern and southeastern semi-arid parts of the RFA region during the Meher growing season. In summary, the median Meher SMD values are 17 %, 30 %, 37 %, and 53 % in humid, sub-humid, dry sub-humid, and semi-arid climates, respectively, while the corresponding median AY values are 93 %, 80 %, 68 % and 46 % (Figure 5Figure 5e, f).
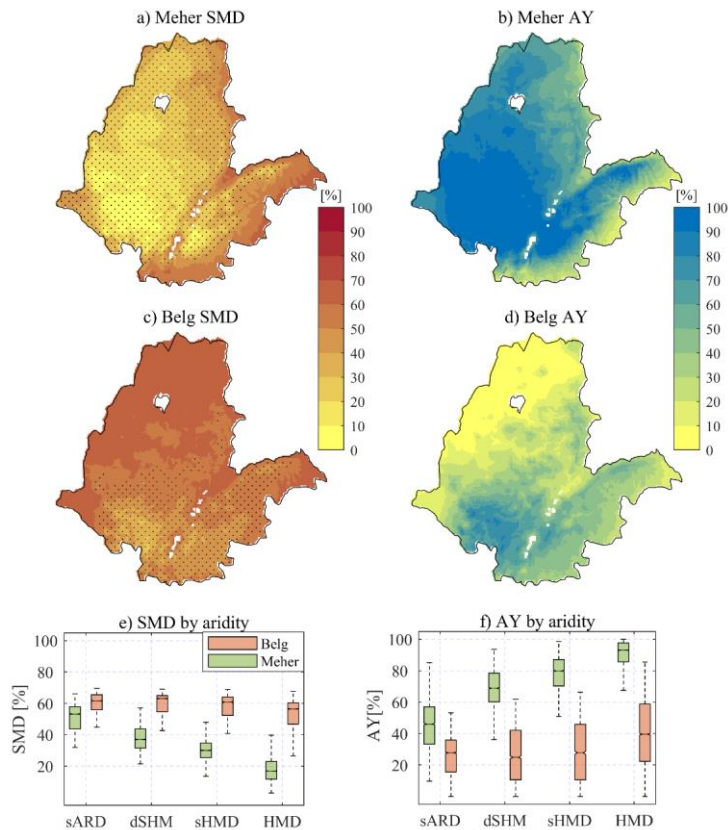
Figure 5: Climatological SMD during Meher (a) and Belg (c), AY for alfalfa grass (Ky = 1.1) during Meher (b) and Belg (d), SMD in different climatic regimes by aridity (e), AY in different climatic regimes during the two growing seasons for the period 1981-2010. Aridity classification is given in Figure 1: sARD = semi-arid, dSMD = dry sub-humid, sHMD = sub-humid, HMD = humid.

365 **The dotted areas in (a) and (c) show the Meher- and Belg-producing regions respectively, delineated based on the Atlas of Ethiopian Rural Socioeconomy (IFPRI and CSA, 2006).**

In the Belg season, the median SMD is mostly below 40 % in the major Belg-producing areas in the south (see Figure 5~~Figure 5~~c), with AY of up to 80 % in the humid areas in the southwestern regions (Figure 5~~Figure 5~~d). In the central and eastern parts of the RFA, which constitute other Belg regions, SMD is higher, reaching up to 60 %, resulting in a correspondingly lower

370 AY of 40-60 %. The northern and northwestern parts of the RFA are dry during the Belg season, thus SMD is very high. Unlike in the Meher season, the differences in SMD among the climatic regimes are less pronounced, with median SMD ranging from 56 % in humid areas and 62 % in semi-arid regions (Figure 5~~Figure 5~~e).
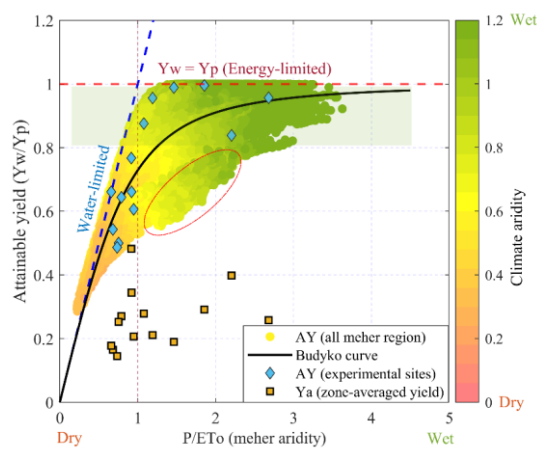
Figure 6: Scatterplot of water-limited attainable maize yield fraction (Yw/Yp) against seasonal aridity showing the energy (dashed

375 **red line) and water limitations (dashed blue line). The color gradient shows the climatic aridity of each grid cell (different from the values on the x-axis, which are seasonal aridity for meher). The solid line represents the parametric Budyko curve fitted to the point cloud. The blue diamonds show Yw at 14 locations across the RFA region, derived from published maize Yp data (fully irrigated, optimally fertilized). The orange squares are the corresponding average actual maize yield (Ya) in the administrative zone within which the experimental location is found. The shaded area indicates maize AY>80 %.**

380

In Figure 6~~Figure 12~~, we presented illustrates the attainable yield (Yw/Yp)~~current conditions of the three yield levels~~ in a Budyko-like space (Budyko, 1958) and included paired Yw (blue diamonds) and Ya (actual yield, orange squares) estimates at 14 locations from previous studies across the RFA region (Table S5) highlight the gaps between these two yield levels for maize. ~~and analyzes the yield gaps with AY.~~ In the Meher season, green water has the potential to produce more than 80 % of

385 Yp across 52 % of the Meher-producing regions of Ethiopia (highlighted by the shaded area in Figure 6Figure 12a). Only about 27 % of the Meher-producing region is moisture-limited (P/ETo < 1). Ya averages only 36% of Yw at the 14 locations, indicating significant potential for yield improvement through enhanced management practices. HoweverNotably, there are areas where the seasonal rainfall is greater than the atmospheric evaporative demand, but AY is still low (e.g., shown by the red ellipse in Figure 12a). This discrepancy explains the non-linearity of the relationship between AY and SMD (shown in

390 Figure S4), which is primarily linked to the combined effects of surfaceclimatic and soil characteristics that influence rainfall-runoff partitioning and green water storage capacity. For example, a low AY for can be associated with sandy soil in a dry climate, while a high AY for the same SMD can be linked to loam soil in a humid climate. From a management perspective, there may be limited options to address inherent soil physical properties like textural composition, apart from measures such as amendment with organic matter, which might to some extent, improve infiltration and green water storage capacity

395 (Hartmann and Six, 2023).

3.3. Future changes in GWA and AY

3.3.1.   Projected changes in growing season rainfall and temperature

Based on the downscaled multiple GCM median projection, the growing season climate across the RFA regions is expected to
400 become warmer and wetter in future periods (Figure 7Figure 6). The temperature increase is progressive over time, especially under the intermediate and high emission scenarios, and shows little spatial variability (e.g., Figure 7Figure 6c). However, changes in rainfall patterns vary across regions and depend on the growing seasons. For example, Meher-producing areas are likely to experience increased rainfall, while dry seasons are expected to remain unchanged or become even drier (e.g., Figure 7Figure 6a, b). Similarly, during the Belg season, the Belg-producing areas in the southern part of the RFA region are expected
405 to become wetter under higher greenhouse gas emissions. In general, a rainfall increase of up to 250 mm (multi-model median with 5-95 percentiles uncertainty ranging from about -150 mm to +850 mm, not shown) is anticipated over a large part of the RFA region during the Meher season under the high emission scenario in the 2060s (Figure 7Figure 6a) and up to 300 mm in the 2080s (not shown). During the Belg season, rainfall increase could reach up to 150 mm (5-95 percentile of about -60 mm to 500 mm) under the high emission scenario in the 2060s. Additionally, the mean annual temperature is projected to rise by
410 up to 3 °C in the 2060s and up to 5 °C by the end of the century.
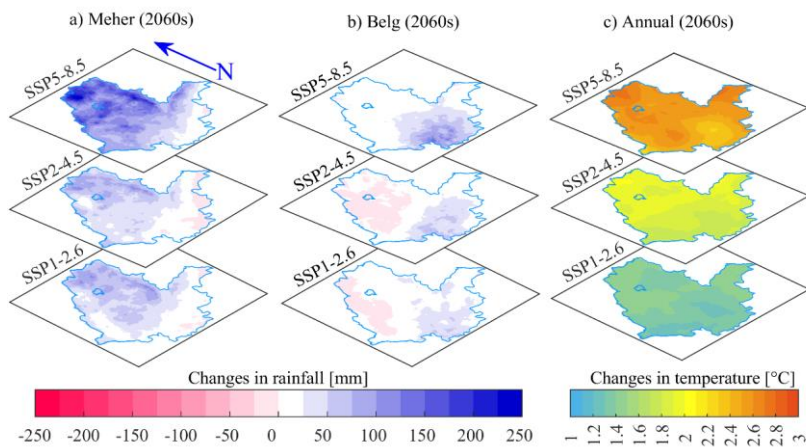
Figure 76: Projected changes in seasonal rainfall in the 2060s during a) Meher (May-September), b) Belg (February-May), and c) changes in annual temperature under the three SSPs. The changes presented here are the median of 26 downscaled GCM projections for rainfall and 21 GCM projections for temperature.

3.3.2. Future changes in soil moisture deficit

In the face of the expected warmer and mostly wetter climate across the RFA region of Ethiopia, the GWA is likely to increase. In the main growing season, Meher, SMD is expected to decrease by up to 5 % over a large part of the region in the 2030s under all emission scenarios (Figure 8Figure 7). However, in the 2060s and 2080s, SMD is projected to increase by 3-15 % over the western, southwestern, and southern parts under the low and intermediate emission scenarios. This is expected, given the projected minimal change in rainfall under the warming climate over these regions, as shown in Fig. 4.6 in the 2060s, for example.
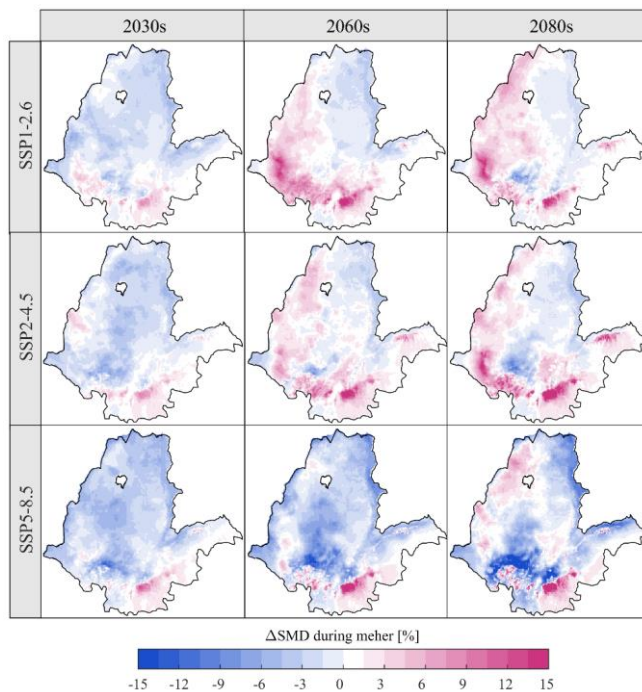
Figure 87: Projected changes in soil moisture deficit (SMD) across the rainfed agricultural region of Ethiopia during the Meher growing season under the SSP1-2.6, SSP2-4.5, and SSP5-8.5 scenarios in the 2030s, 2060s, and 2080s.

425   Under the high emission scenario, soil moisture deficit is likely to decrease over the majority of the region, following the increase in rainfall. The central and northeastern parts of the RFA regions are generally expected to experience a slight decrease in SMD and thus slightly higher GWA under all scenarios in the future. The highest increase in SMD was observed in the southwestern and southern parts of the RFA region, where the Meher rainfall mostly remains unchanged (see Figure 7Figure 6a).

430   In the Belg growing season, soil moisture deficit consistently decreases over the producing regions in the future periods under all scenarios (Figure 8). These increases in GWA are particularly significant across the main Belg region in the southwestern parts of the RFA. In these areas, SMD is expected to decrease by up to 6 % in the 2030s (2020-2049) and by over 15 % in the 2080s under the low and intermediate emission scenarios.
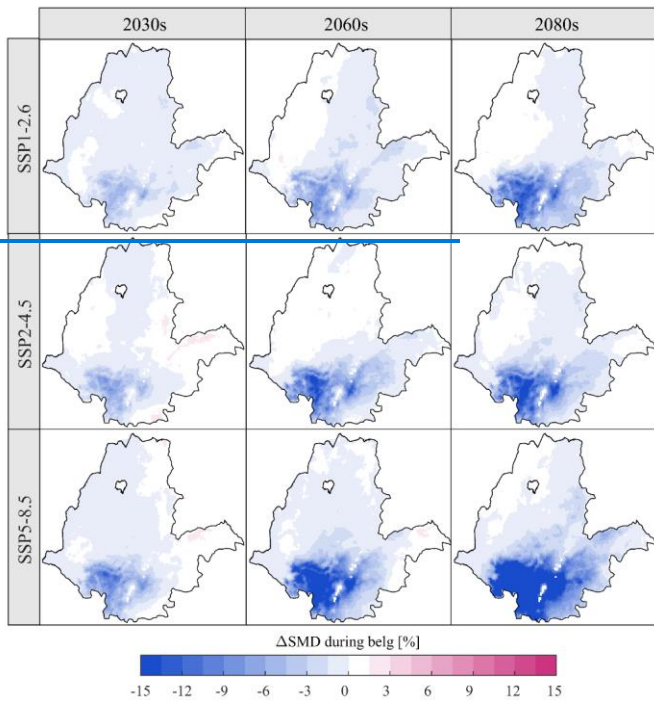
435 Figure 8: Projected changes in soil moisture deficit (SMD) across the rainfed agricultural region of Ethiopia during the Belg growing season under the SSP1-2.6, SSP2-4.5, and SSP5-8.5 scenarios in the 2030s, 2060s, and 2080s

Under the high emission scenario, GWA across the primary Belg-producing regions in the south and southwest is expected to increase by up to 23 % by the end of the century.

Overall, the projected changes in soil moisture deficit across the study area are largely consistent with a recent global-scale
440 assessment by Liu et al. (2022), which reported a decrease in agricultural water scarcity of up to 15 % in the RFA region for a comparable future period (2026-2050) and reference period (1981-2005) under the RCP2.6 scenario.

3.3.3. Future changes in water-limited crop yields

The likely implications of changes in SMD on attainable yields for the four major cereal crops (teff, maize, sorghum, wheat)

445 cultivated in Ethiopia are presented next. We summarize the changes occurring during the two growing seasons in their respective producing regions (Wakjira, 2024) and across the various climatic regimes of the RFA.
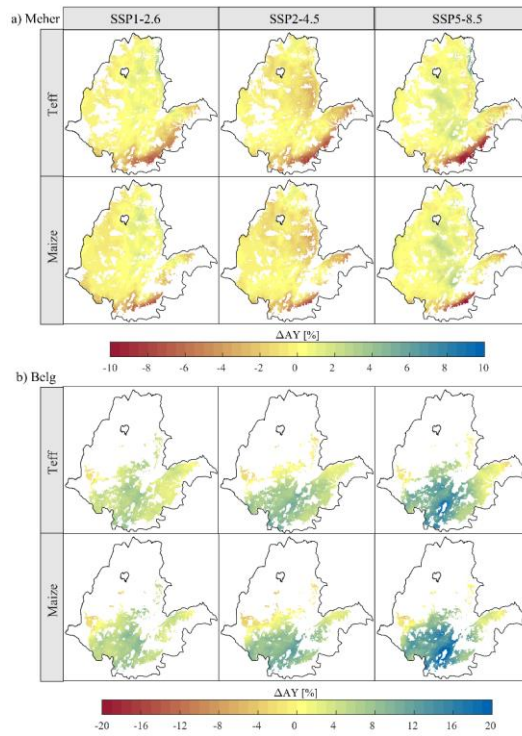
Figure 99: Projected changes in water-limited attainable yield for teff and maize in Meher (a) and Belg (b) during the 2060s under the SSP1-2.6, SSP2-4.5, and SSP5-8.5. The RFA region was masked using cropland suitability maps (Wakjira et al., under review)
450 **to restrict the analysis to areas potentially suitable for each crop. The non-producing areas during both seasons were also masked out following the Atlas of Ethiopian Rural Socioeconomy (IFPRI and CSA, 2006).**

455 **Meher season**

In the Meher season, minor or no changes in AY are expected, although regional differences exist in both the magnitude and direction of these changes. For example, for the 2060s, the projected changes in AY for teff range from -7.8 % to 5.3 % under the low-emission scenario, and from -12.1 % to 10.7% under the high-emission scenario. Similarly, for maize, the expected changes range from -7.8 % to 4.7 % under the ~~low~~ low-emission scenario, and from -11.5 % to 6 % under the ~~high~~ high-

460 emission scenario (Figure 9~~Figure 9~~a). Under the intermediate emission scenario, the changes are predominantly negative, ranging from -9.3 % to 1.8 % for teff and from -8.2 % to 1.2 % for maize. Similar order of magnitude and direction of changes were observed for sorghum and wheat crops (refer to Figure~~.~~ ~~S3~~S6-~~7~~9).

Comparing the near- and long-term future changes, we note a decreasing trend in AY for all crops under all emission scenarios. During the 2030s, the northern parts of the RFA region are likely to experience increases, while decreases are mainly evident

465 in the southern and southeastern parts of the Meher-producing areas. Notably, the marginal areas in the south and southeast are likely to experience the most significant decrease in AY for all crops and under all scenarios. By the 2080s, most Meher-producing areas are expected to witness either no change or a decrease in AY (Figure~~.~~ ~~S3~~S6-~~7~~9).

We also examined the water-limited attainable yield responses in different climatic regimes (Figure 10~~Figure 10~~). In humid areas, the temporal changes and spatial variability in AY are small for all crops under all emission scenarios. This is because

470 these areas rarely have moisture limitations, meaning that an increase in rainfall will have a minimal effect on yield improvement. In contrast, in semi-arid, dry sub-humid, and sub-humid areas, AY is likely to increase in the 2030s and then consistently decrease in future periods under both low and high emission scenarios. Under the intermediate scenario, AY is expected to decrease in the 2060s and then increase in the 2080s. Spatial variations are particularly high for teff, especially in semi-arid areas with changes ranging from -10 % to +5 % in the 2060s.

475 **Belg season**

Following the increased rainfall and the subsequent rise in GWA, AY is projected to increase significantly and progressively over the major parts of the Belg-producing regions in future periods. However, a few areas will experience small decreases (Figure 9~~Figure 9~~b). For teff, the expected changes in the 2060s range from -3.5 % to 8.8 % under the ~~low~~ low-emission scenario and from -3.6 % to 21.7 % under the ~~high~~ high-emission scenario. Similarly, for maize, the changes range from -5.9

480 % to 10.6 % under the low-emission scenario and from -4.7 % to 27.6 % under the high-emission scenario. These positive changes are expected to intensify, particularly under the ~~high~~ high-emission scenario, with the majority of the Belg-producing region experiencing an increase in AY of over 20 % for all crops examined. The changes for all crops and future periods have been illustrated in the supplementary material appended to this paper (Figure~~.~~ ~~S7~~S10-~~10~~13).

485
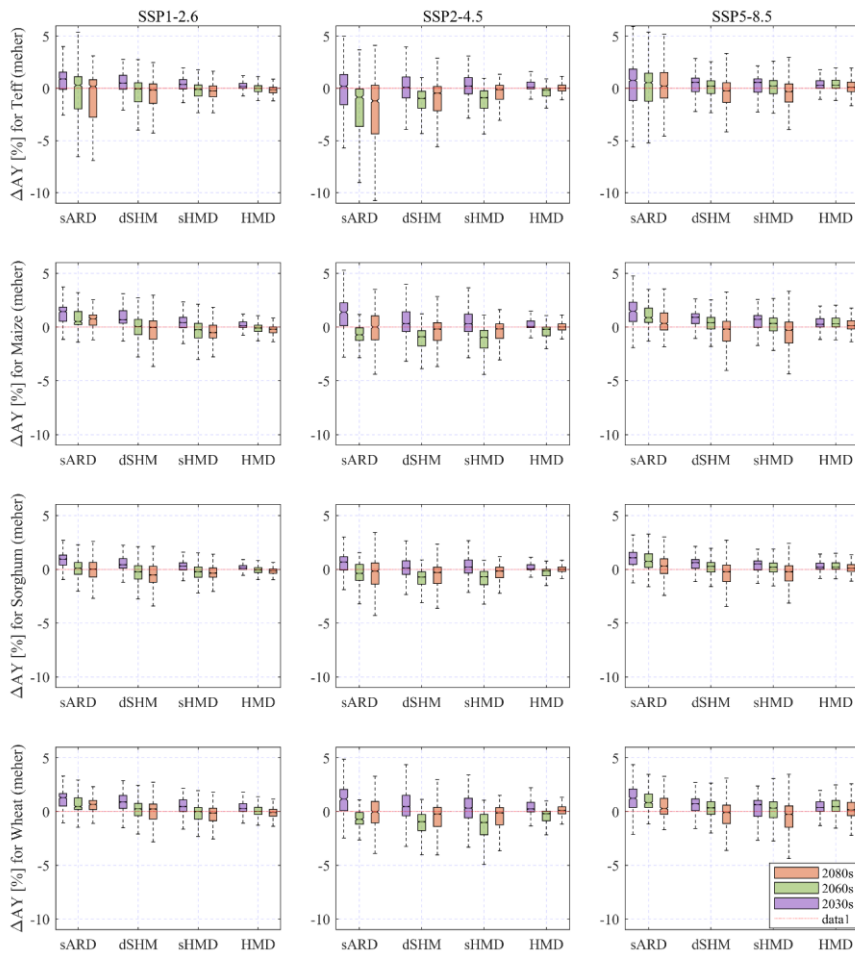
Figure 1010: Boxplots of the projected changes in water-limited yields (AY) of the four major cereal crops produced in Ethiopia in different climatic regimes under the three SSPs during the three future periods, during the Meher growing season. Each boxplot represents the distribution of AY changes within Meher-producing areas for all grid cells in the respective climatic regime. Outlier values have been excluded.

490

The changes in AY during the Belg season in different climatic regimes are illustrated in Figure. S11S14. The variations in overall changes in AY among these regimes depend on the emission scenario. Under the low emission scenario, median changes in AY do not significantly vary across climatic regimes, remaining positive throughout the three future periods for all crops examined. In contrast, under the intermediate and high high-emissions, AY tends to increase with climatic wetness (from semi-arid to humid climates).

Decreases in AY are mainly noticeable in semi-arid and dry sub-humid areas in the 2030s, particularly under the intermediate emission scenario. However, during the 2060s and 2080s, median changes in AY are positive and relatively consistent across climatic regimes for all crops. The projected increases in AY are higher for maize and wheat compared to teff and sorghum. Spatial variability in changes generally increases with climatic wetness and into the future periods under the low low-emission scenario while a decreasing pattern rarely observed under the intermediate and high high-emission scenarios. In all cases, spatial variability of the changes is lower in the 2030s compared to the mid- and long-term future periods. Concerning the examined crops, it was observed that the projected increases in AY are higher for maize and wheat compared to teff and sorghum.

3.3.4. Climate sensitivity of attainable crop yields

The spatiotemporal average relative sensitivity (β_{ratio}) of AY to atmospheric evaporative demand (AED) and rainfall for the four crops under the three SSPs are presented in Figure 11Figure 11. The results are averaged for the three future periods for the main growing season Meher at the administrative agricultural zones of Ethiopia. Results for the Belg short growing season are presented in Figure. S12S15. The climate sensitivity is reported at a zonal scale, rather than at the grid scale, to provide zone-specific insights into the relative importance of ETo and rainfall that determines future green water supply; this information is crucial for agricultural water management planning, service provision, and decision-making at the institutional scale. For the interpretation, we categorize the sensitivity of AY as AED-sensitive ($\beta_{ratio} \leq 0.8$), AED- and rainfall-sensitive ($0.8 < \beta_{ratio} < 1.2$), and rainfall-sensitive ($\beta_{ratio} \geq 1.2$).

During the Meher growing season, AY is predominantly AED-sensitive for all crops under all emission scenarios we considered (Figure 11Figure 11). The percentage of zones across which AY is, on average, AED-sensitive is 64 % for teff, 50 % for maize, 52 % for sorghum and 77 % for wheat under low emissions. The influences of AED on AY increase with GHG emissions. Under high emissions, AED dominates the changes in AY in 82 %, 65 %, 73 %, and 92 % of the zones for teff, maize, sorghum, and wheat respectively. In the remaining zones, the simultaneous influences of rainfall and AED are evident, except for maize, where rainfall has a more significant impact than AED. Notably, changes in rainfall have a low influence on teff and wheat, with AY being rainfall-sensitive in less than 5 % of the zones. These crops are exceptionally more sensitive to AED compared to maize and sorghum, as indicated earlier. Temporal changes in climate sensitivity of AY are also evident, but the spatial patterns do not change significantly in future periods.

The influences of changes in AED and rainfall on AY are primarily linked to the climatic regimes of the RFA region. In semi-arid and dry sub-humid climates, AY is predominantly AED-sensitive. This is particularly noticeable in the northeastern zones (covering the eastern parts of Tigray and Amhara, and western zones of Afar regions) and the central to eastern zones (including East Shoa, Arsi, and Hararge zones of the Oromia region) in the RFA region for all crops under low emissions (left panels in Figure 11Figure 11). This influence of AED intensifies to more zones in sub-humid and humid climates under the intermediate and high emissions. Rainfall-sensitivity is largely evident in humid climates, mostly in the central, western, and northwestern zones under low emissions for all crops except wheat, which is rainfall-sensitive only in the northwestern parts of the RFA region (Western Tigray and North Gonder zones). Maize AY is strongly rainfall-sensitive under all scenarios, across the humid zones in the western part of Oromia (Wollega, Jimma, and Illubabor zones), Sidama region, and most of the zones of the SNNP region in the southwestern part.

In contrast to the main growing season, future changes in AY during the Belg growing season are primarily influenced by changes in rainfall, particularly in the main Belg-producing areas in the southwestern, southern, and southeastern parts of the RFA region for all crops under all SSPs (Figure. S12S15). There is less spatio-temporal change in the rainfall sensitivity of Belg AY. Only under the high emission scenario does the influence of changes in AED contribute to the influences of rainfall, primarily in the northern half of the RFA region, which remains dry during this season.
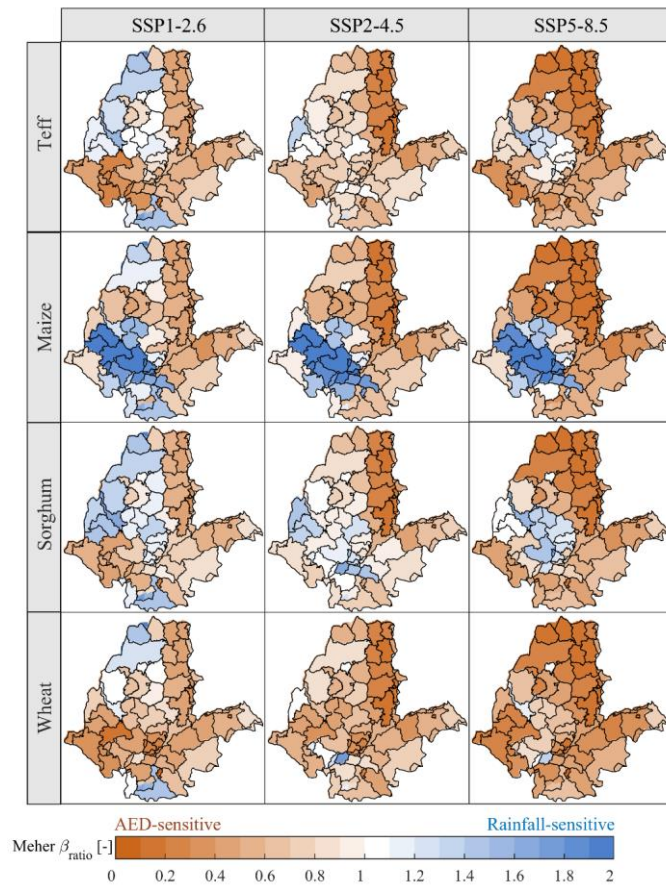
Figure 11: Area-averaged relative sensitivity (β_ratio) of water-limited attainable yields (AY) to rainfall and atmospheric evaporative demand (AED) for the Meher growing season at the administrative zone level under the low, intermediate, and high emission scenarios. The mapped values represent the average of β_ratio of all grid cells within each zone, and all three future periods. The names of the administrative zones are indicated in Figure 1 and Table S1.

4. Discussion

4.1. ~~Current~~ Future green water limitations and crop yield~~s~~ ~~gaps~~in Ethiopia

Achieving crop yield at its potential level is not only a matter of adaptation to climate variability and change, but it is also a key strategy for eradicating rural poverty and building resilience in heavily agricultural nations like Ethiopia (Abrams, 2018; Tittonell and Giller, 2013). ~~In the effort to enhance crop yields, three levels of yields can be defined and targeted (van Ittersum et al., 2013): (i) potential yield (Yp), primarily defined by temperature, radiation, light, and cultivar; (ii) water-limited yield (Yw), determined by moisture availability and soil type, but within the constraints of Yp; and (iii) actual yield (Ya), which is dependent mainly on farm management practices including water, soil, nutrient, pest and weed management.~~ In RFA systems green water is a major limiting factor, and thus, Yw defines the rainfed crop yield potential (Dijk et al., 2017; van Ittersum et al., 2013)~~.~~, ~~as Yp can be reached only by supplementing the green water through irrigation to fully meet the crop water demand.~~ Our analysis sheds a broader light on the potential of green water for crop production, its spatial variability, and temporal changes (at climatological timescale) in the face climate change in across the RFA region of Ethiopia.

We showed that the likely wetting and warming climate across the large part of the Ethiopian RFA region is expected to slightly enhance green water availability (GWA) in the near future. This is largely consistent with a recent global-scale assessment by Liu et al. (2022), which reported a decrease in agricultural water scarcity of up to 15 % in the RFA region for a comparable future period (2026-2050) and reference period (1981-2005) under the RCP2.6 scenario. However, it is also evident that in the long term, the effects of climate warming outweigh those of climate wetting, leading to green water scarcity. For example, ~~(~~Setegn et al.~~,~~ (2011) in a SWAT-based evaluation of future agricultural water availability in the Lake Tana basin in northern Ethiopia using four GCMs, revealed a decreasing tendency in soil moisture (by up to -2%) during the mid and end of the century, which aligns with our estimates for that area (-3% to +1.5%, Figure 5). In the northeastern semi-arid areas, GWA is expected to improve under all emission scenarios, across all future periods, and in both growing seasons. This is consistent (in terms of the direction of change) with another recent assessment based on the SWAT+ model driven by multiple GCM projections under medium and high emission scenarios, which reported substantial increases in GWA in future periods in the Kobo-Golina River catchment (Abate et al., 2024). Similarly, our findings in the central Rift Valley support those of ~~(~~Muluneh, (2020), who reported increases in soil moisture based on AquaCrop model for maize forced by ensemble GCM projections under the high emission scenario. The observed decreases in GWA across the southeastern semi-arid areas is the combined effects the no change or drying tendency, and temperature warming. Our findings in this area contradicts with those of ~~(~~Serur, (2020), which predicts increases in GWA in Weyn River catchment.

It has been widely reported that crop yield across the tropics, including East Africa, are likely negatively affected by climate change (e.g., Asseng et al., 2015; Jägermeyr et al., 2021; Li et al., 2022; Rosenzweig et al., 2014). We observe overall decreasing tendencies in Meher season AY for the four crops studied, across all climatic regimes, under all emission scenarios by the mid and end of the century (Figure 10). In this regard, our results align with a recent study by (Yang et al., 2023), which

assessed climate-driven changes in maize yields in Ethiopia using the process-based DSSAT model with four GCM projections and similarly indicated a decreasing trend in yields. Our findings also align with the work of (Rettie et al., (2022), which used an ensemble of crop models and similarly concluded decreases in Meher maize and wheat yields by mid-century. Consistent with our findings (Figure 11), they also reported that maize and wheat yields are more sensitive to temperature changes than to changes in rainfall. In Gambella, western Ethiopia, (Degife et al., (2021) observed a decreasing trend in maize yields
580   throughout the 21st century, with temperature playing a strong role in driving the change, which aligns with our findings except for the 2030s, for which we found no change or a slight increase (Figure S8). Additionally, the projected slight increases in maize AY in Bako (central west) and slight decreases in Melkasa (central east) are comparable to those of (Araya et al., (2015). However, our findings largely contradict the crop yield projections based on a statistical model forced by two regional climate model projections (Kassaye et al., 2021), which reported substantial increases in teff and maize yields and substantial decreases
585   for sorghum and wheat.

Figure 12 illustrates the current conditions of the three yield levels in a Budyko-like space (Budyko, 1958) and analyzes the yield gaps with AY. In the Meher season, green water has the potential to produce more than 80 % of Yp across 52 % of the Meher-producing regions of Ethiopia (highlighted by the shaded area in Figure 12a). Only about 27 % of the Meher-producing
590   region is moisture-limited (P/ETo < 1). However, there are areas where the seasonal rainfall is greater than the atmospheric evaporative demand, but AY is still low (e.g., shown by the red ellipse in Figure 12a). This discrepancy is primarily linked to surface and soil characteristics that influence rainfall-runoff partitioning and green water storage capacity. From a management perspective, there may be limited options to address inherent soil physical properties like textural composition, apart from measures such as amendment with organic matter, which might to some extent, improve infiltration and green water storage
595   capacity (Hartmann and Six, 2023).

Field Code Changed

Field Code Changed

Field Code Changed

4.2. Uncertainties and limitations

From the model evaluation (Section 3.1), it is evident that the CHC modelling framework can reliably estimate the agrohydrological variables at a grid scale with minimal complexity for our stated purpose, which is to inform long-term agricultural water management, climate adaptation, resilience, and rural economic development in Ethiopia. Before we further discuss the practical implications of the GWA and AY conditions across the RFA region, we first highlight the limitations of the CHC model structure, especially the considerations needed when applying the model in different contexts, particularly in terms of purpose and temporal scale.

One of the simplifications in the CHC modelling framework is the use of the CN-based soil water balance model. The main limitation of the method stems from the empirical parameters – namely the curve number, and initial abstraction ratio, used to simulate the vertical soil water balance at grid scale without routing the surface as well as subsurface flow. Therefore, these parameters must be properly calibrated for site-specific conditions (Assaye et al., 2021; Qi et al., 2020), particularly when the model is applied at local scale and shorter time scale. In our application, calibration over the entire RFA region is rather difficult as this would require large local observation data.

We quantified the uncertainty associated with the CN-based rainfall-runoff partitioning approach (CHC-CN) by comparing it to a water balance model that is based on the maximum soil infiltration capacity (CHC-WB), another widely applied concept (e.g., Chiarelli et al., 2020; Hoogeveen et al., 2015; Sishu et al., 2024; Tenreiro et al., 2020). In CHC-WB we assumed that surface runoff events occur when rainfall on a given day exceeds the maximum infiltration capacity (the difference between water content at saturation, and soil water content on the day before). Comparing the AY simulated using CHC-CN and CHC-WB, we found negligible differences between the models (Figure 12), with root mean squared deviation (RMSD) from the observed AY of 10.98 % for CHC-CN and 10.86 % for CHC-WB. Similarly, the differences in ETa and SMD simulated by the two models were small (see Figure S16b and c). The main discrepancy appeared in surface runoff (Q) and deep percolation (Dp) simulations (Figure S16a), as the CHC-WB model does not adequately differentiate surface and subsurface flow, diverting a larger portion of runoff to deep percolation. Although both surface runoff (Q) and deep percolation (Dp) are not the primary variables of interest in our analysis, their accurate estimation is crucial for other agrohydrological applications, such as water harvesting, flood (spate) irrigation design, and agricultural drainage system design, and monitoring soil and nutrient erosion. When input parameters like rainfall intensity and infiltration characteristics are available, and the model's complexity is manageable, infiltration-based models, such as those using Richards' equation (Richards, 1931) may provide more precise results than the curve number and water balance-based models.
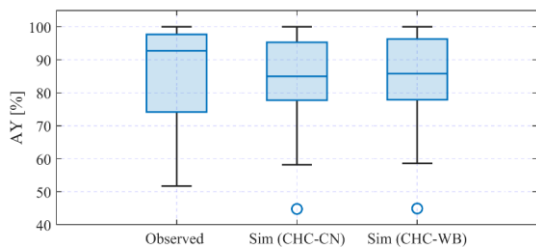
Figure 12: Comparison of CHC-simulated AY using the CN-based and water balance (WB)-based rainfall-runoff partitioning methods at 45 locations (Table S4) for which independent (observed) AY were collected published field trials, crop model simulations and GYGA (www.yieldgap.org).

The crop module of the CHC modelling framework estimates relative crop yield only at a seasonal scale using the evaporative stress index (ESI) as a climatic factor and the yield response factor (Ky) to represent the seasonal crop response. In crop and agroecosystem modelling, such models are categorized as crop coefficient models and are primarily used for planning and decision-making (Foster and Brozović, 2018; He et al., 2022; Schwartz et al., 2020). Sub-seasonal variabilities of stress conditions (water, thermal, light, nutrient, etc) as well as the crop physiological responses within the growing, season have not been represented in the CHC modelling framework. Therefore, the use of the framework should not aim for accurate simulation of crop growth and yields; such simulations should be based on process-based crop models, which are capable of accounting

for major influences of climate change such as the negative effects of heat stress and the positive effects of elevated CO_2 on future crop yield (Becker et al., 2023; Lobell et al., 2011b). In our analysis, which focuses on assessing changes on a climatological timescale, we focused on the rainy seasons (May to September, and February to May) climate and instead of accurately defining the growing period from planting to harvest. While the uncertainties associated with the choice of growing period are averaged out at climatological times scale, accurate planting date is an important input in process-based crop growth and yield simulations at local and sub-seasonal scales (Lala et al., 2021).

Despite the uncertainties and limitations outlined, the results presented are robust and offer valuable insights for practitioners in planning and policy formulation in Ethiopia. Furthermore, the model developed can be adapted for application in different regions and climates, enhancing its utility for broader decision-making processes.

4.3. Implications for green water management and sustainable intensification

While the changes in water-limited attainable yield vary greatly across the RFA in terms of both magnitude and direction during the main growing season, the results show that semi-arid and dry sub-humid areas are most likely to experience a reduction in AY. On one hand, this is attributed to an intensified soil moisture deficit, as evident for example in the northwestern, western, southern, and southeastern semi-arid areas (with low and intermediate emissions in the 2060s and 2080s, in Figure 8Figure 6), and on the other hand, it is also a result of increases in AED-sensitivity (Figure 11Figure 11), particularly in the moisture-limited regions. In these regions, it would be beneficial to implement on-farm water management strategies that maximize green water availability and minimize non-productive green water flows.

Practices that aim to maximize GWA should focus on altering the rainfall-runoff partitioning processes by increasing the opportunity for infiltration during rainfall through various surface management practices. For example, tillage and physical measures like bunds, infiltration trenches, tied-ridge, and planting pits among others (Hurni, 2016; Makurira et al., 2009; Nyakudya et al., 2014) have been successfully evaluated in field experiments and on-farm practices. Other measures like residue retention and cover cropping not only enhance infiltration, but also suppress the non-productive evaporation from the soil surface. (Rockström, 2003). Additionally, measures that improve infiltration also offer the side benefit of reducing soil erosion by runoff, another critical challenge that contributes to the crop yield gap. Finally, we strongly suggest that the selection of water management practices should be carefully made by evaluating their need and suitability primarily based on climate and soil characteristics. For example, in humid climates with heavy clay soils, such practices may result in waterlogging problems, which is also a major yield-reducing factor in such environments (Manik et al., 2019; Pittelkow et al., 2015).

4.3. Intensification of the Belg season production

The projected increase in GWA and AY during the Belg season may provide an additional opportunity for farmers to intensify their production during this season. This, however, will need firm stakeholder commitment to plan and mobilize resources for action in the framework of National Adaptation Plans (NAP) and similar initiatives (Conway and Vincent, 2021). Long-term awareness of stakeholders, ranging from the institutional level to farm-level actors, on the expected challenges and

opportunities of climate change, supported by climate information services for short-term decisions, is highly important to exploit such opportunities (Grossi and Dinku, 2022). In addition to climate information like the forecast information of the expected onset and cessation of Belg rain, extensive support on proper selection of crop types compatible with the duration of the short growing season is vital to help farmers effectively plan and undertake bi-annual production without compromising the main growing season.

5. Conclusions

We investigated the cascading effects of climate on green water availability and water-limited attainable yield (AY) in the context of the rainfed agricultural region of Ethiopia. We integrated hydroclimatic processes with crop yield response through an agrohydrological modelling framework to assess the current potential, future changes, and climate sensitivity of AY. The AY across the Ethiopian RFA region is 79 % of what could be produced under water-unlimited conditions during the main growing season (Meher) and 37 % during the shorter season (Belg) during the reference period, with regional variation depending on the climatic regimes. The soil moisture deficit (percent of soil moisture content at field capacity) during this period is on average about 29 % in Meher and 56 % in Belg.

The future climate over the RFA region is expected to be warmer and mostly wetter. Under these changes, future changes in green water availability and AY vary across regions, emission scenarios, future periods, and between the two growing seasons. In Meher, the expected changes in AY range largely in the ±5 % range under all scenarios and future periods. Changes during the 2030s are largely positive under all scenarios, but AY shows overall decreases in the 2060s and 2080s. Decreases in AY are mostly evident in semi-arid regions, with teff being the most affected. These changes are dominantly driven by the atmospheric evaporative demand (AED), that is by temperature increase, especially in moisture-limited regions. The influence of AED increases under the intermediate and high emission scenarios, suggesting the need for due attention to management strategies that suppress evaporative losses in the future. In Belg, AY is expected to progressively increase by up to 20 % under the high emission scenario by the end of the century, providing an opportunity for farmers to expand crop production in this season. These changes are dominantly driven by increases in rainfall, implying that green water management practices that increase water availability would further improve crop yields during this season. Furthermore, our assessment of documented field experiment results and crop yield data from the RFA region reveals a large gap between the actual and water-limited yield. For example, for maize on average only 36 % of AY is actually realized under the current practices, suggesting that green water management practices should be combined with other measures that overcome the yield-reducing factors related to soil nutrient, tillage practices, plant protection, and cultivar improvement.

Finally, the CHC modeling framework developed in this study can be applied to conduct similar assessments in other regions. It can also be adopted for various agrometeorological applications, such as estimating seasonal water availability and crop water demand for both irrigated and rainfed systems, as well as predicting relative yields for management planning and

decision-making. The~~is~~ framework minimizes dependence on process-based crop models for such analyses, which often require intensive measurement data for the calibration of several model parameters.

710 **Data availability**: The processed data and simulation output will be made available upon request.

Author contribution: Conceptualization: MTW; Data curation: MTW; Modelling and analysis: MTW; Methodological and result discussions: MTW, NP, JS, PM; Darft preparation: MTW; Revision: NP, JS, PM; Supervision: PM

Competing interests: At least one of the (co-)authors is a member of the editorial board of Hydrology and Earth System Sciences. The authors have no other competing interests.

715 **Acknowledgments**

We thank Silvan Ragettli for his valuable comments and suggestions on the evapotranspiration data and outputs. MTW was supported by ETH for Development (ETH4D), ETH Zurich, through the E4D Doctoral Scholarship Program. NP was supported by the Swiss National Science Foundation (SNSF), Grant 194649 ("Rainfall and floods in future cities").

720 **References**

Abate, B. Z., Alaminie, A. A., Assefa, T. T., Tigabu, T. B., and He, L.: Modeling climate change impacts on blue and green water of the Kobo-Golina River in data-scarce upper Danakil basin, Ethiopia, J. Hydrol. Reg. Stud., 53, https://doi.org/10.1016/j.ejrh.2024.101756, 2024.

Abatzoglou, J. T., Dobrowski, S. Z., Parks, S. A., and Hegewisch, K. C.: Data Descriptor : TerraClimate , a high-resolution
725 global dataset of monthly climate and climatic water balance from 1958 – 2015, 1–12, 2017.

Abera, K., Crespo, O., Seid, J., and Mequanent, F.: Simulating the impact of climate change on maize production in Ethiopia, East Africa, Environ. Syst. Res., 7, https://doi.org/10.1186/s40068-018-0107-z, 2018.

Abrams, L.: Unlocking the potential of enhanced rainfed agriculture, Stockholm, 2018.

Adam, M., Van Bussel, L. G. J., Leffelaar, P. A., Van Keulen, H., and Ewert, F.: Effects of modelling detail on simulated
730 potential crop yields under a wide range of climatic conditions, Ecol. Modell., 222, 131–143, https://doi.org/10.1016/j.ecolmodel.2010.09.001, 2011.

Allen, R. G., Pereira, L. S., Raes, D., and Smith, M.: Crop Evapotranspiration, Irrigation and Drainage Paper No. 56, Rome, 326 pp., 1998.

Anandhi, A., Frei, A., Pierson, D. C., Schneiderman, E. M., Zion, M. S., Lounsbury, D., and Matonse, A. H.: Examination of
735 change factor methodologies for climate change impact assessment, 47, 1–10, https://doi.org/10.1029/2010WR009104, 2011.

Araya, A., Stroosnijder, L., Girmay, G., and Keesstra, S. D.: Crop coefficient, yield response to water stress and water productivity of teff (Eragrostis tef (Zucc.), Agric. Water Manag., 98, 775–783, https://doi.org/10.1016/j.agwat.2010.12.001, 2011.

Araya, A., Girma, A., and Getachew, F.: Exploring Impacts of Climate Change on Maize Yield in Two Contrasting Agro-Ecologies of Ethiopia, Asian J. Appl. Sci. Eng., 4, 2305–915, 2015.

Assaye, H., Nyssen, J., Poesen, J., Lemma, H., Meshesha, D. T., Wassie, A., Adgo, E., and Frankl, A.: Curve number calibration for measuring impacts of land management in sub-humid Ethiopia, J. Hydrol. Reg. Stud., 35, 100819, https://doi.org/10.1016/j.ejrh.2021.100819, 2021.

Asseng, S., Ewert, F., Martre, P., Rötter, R. P., Lobell, D. B., Cammarano, D., Kimball, B. A., Ottman, M. J., Wall, G. W., White, J. W., Reynolds, M. P., Alderman, P. D., Prasad, P. V. V., Aggarwal, P. K., Anothai, J., Basso, B., Biernath, C., Challinor, A. J., De Sanctis, G., Doltra, J., Fereres, E., Garcia-Vila, M., Gayler, S., Hoogenboom, G., Hunt, L. A., Izaurralde, R. C., Jabloun, M., Jones, C. D., Kersebaum, K. C., Koehler, A. K., Müller, C., Naresh Kumar, S., Nendel, C., O'leary, G., Olesen, J. E., Palosuo, T., Priesack, E., Eyshi Rezaei, E., Ruane, A. C., Semenov, M. A., Shcherbak, I., Stöckle, C., Stratonovitch, P., Streck, T., Supit, I., Tao, F., Thorburn, P. J., Waha, K., Wang, E., Wallach, D., Wolf, J., Zhao, Z., and Zhu, Y.: Rising temperatures reduce global wheat production, Nat. Clim. Chang., 5, 143–147, https://doi.org/10.1038/nclimate2470, 2015.

Becker, R., Schüth, C., Merz, R., Khaliq, T., Usman, M., Beek, T. aus der, Kumar, R., and Schulz, S.: Increased heat stress reduces future yields of three major crops in Pakistan's Punjab region despite intensification of irrigation., Agric. Water Manag., 281, 108243, https://doi.org/10.1016/j.agwat.2023.108243, 2023.

Bieger, K., Arnold, J. G., Rathjens, H., White, M. J., Bosch, D. D., Allen, P. M., Volk, M., and Srinivasan, R.: Introduction to SWAT+, A Completely Restructured Version of the Soil and Water Assessment Tool, J. Am. Water Resour. Assoc., 53, 115–130, https://doi.org/10.1111/1752-1688.12482, 2017.

Borgomeo, E., Khan, H. F., Heino, M., Zaveri, E., Kummu, M., Brown, C., and Jägerskog, A.: Impact of green water anomalies on global rainfed crop yields, Environ. Res. Lett., 15, https://doi.org/10.1088/1748-9326/abc587, 2020.

Buchhorn, M., Smets, B., Bertels, L., De Roo, B., Lesiv, M., and Tsendbazar, Nandin-Erdene Tarko, A.: Copernicus Global Land Operations "Vegetation and Energy" "CGLOPS-1," Copernicus Glob. L. Oper., 1–93, https://doi.org/10.5281/zenodo.3938963.PU, 2020.

Budyko, M. I.: The Heat Balance of the Earth's Surface, 1958.

Burke, M. B., Lobell, D. B., and Guarino, L.: Shifts in African crop climates by 2050, and the implications for crop improvement and genetic resources conservation, Glob. Environ. Chang., 19, 317–325, https://doi.org/10.1016/j.gloenvcha.2009.04.003, 2009.

Čerkasova, N., White, M., Arnold, J., Bieger, K., Allen, P., Gao, J., Gambone, M., Meki, M., Kiniry, J., and Gassman, P. W.: Field scale SWAT+ modeling of corn and soybean yields for the contiguous United States: National Agroecosystem Model Development, Agric. Syst., 210, https://doi.org/10.1016/j.agsy.2023.103695, 2023.

770 Chiarelli, D. D., Passera, C., Rosa, L., Davis, K. F., D'Odorico, P., and Rulli, M. C.: The green and blue crop water requirement WATNEEDS model and its global gridded outputs, Sci. Data, 7, 1–9, https://doi.org/10.1038/s41597-020-00612-0, 2020.

Conway, D. and Vincent, K.: Conversations About Climate Risk, Adaptation and Resilience in Africa, 147–162 pp., https://doi.org/10.1007/978-3-030-61160-6_9, 2021.

CSA: Summary and statistical report of the 2007 population and housing census, Addis Ababa, 113 pp., 2007.

775 CSA: Agricultural sample survey (2010/2011): Report on area and production of crops, Central Statistical Agency, Addis Ababa, Ethiopia, 2010.

Degife, A. W., Zabel, F., and Mauser, W.: Climate change impacts on potential maize yields in Gambella Region, Ethiopia, Reg. Environ. Chang., 21, https://doi.org/10.1007/s10113-021-01773-3, 2021.

van Diepen, C. A., Wolf, J., van Keulen, H., and Rappoldt, C.: WOFOST: a simulation model of crop production, Soil Use 780 Manag., 5, 16–24, https://doi.org/10.1111/j.1475-2743.1989.tb00755.x, 1989.

Dijk, M. Van, Morley, T., Jongeneel, R., Ittersum, M. Van, Reidsma, P., and Ruben, R.: Disentangling agronomic and economic yield gaps : An integrated framework and application, Agric. Syst., 154, 90–99, https://doi.org/10.1016/j.agsy.2017.03.004, 2017.

Doorenbos, J. and Kassam, A. H.: Paper 33. Yield Response to water, FAO Irrigation and Drainage Paper, 203 pp., 1979.

785 Dorigo, W., Wagner, W., Albergel, C., Albrecht, F., Balsamo, G., Brocca, L., Chung, D., Ertl, M., Forkel, M., Gruber, A., Haas, E., Hamer, P. D., Hirschi, M., Ikonen, J., de Jeu, R., Kidd, R., Lahoz, W., Liu, Y. Y., Miralles, D., Mistelbauer, T., Nicolai-Shaw, N., Parinussa, R., Pratola, C., Reimer, C., van der Schalie, R., Seneviratne, S. I., Smolander, T., and Lecomte, P.: ESA CCI Soil Moisture for improved Earth system understanding: State-of-the art and future directions, Remote Sens. Environ., 203, 185–215, https://doi.org/10.1016/j.rse.2017.07.001, 2017.

790 Falkenmark, M.: The New Blue and Green Water Paradigm : Breaking New Ground for Water Resources Planning and Management, 132, 129–132, https://doi.org/10.1061/(ASCE)0733-9496(2006)132, 2006.

Fan, J., McConkey, B., Wang, H., and Janzen, H.: Root distribution by depth for temperate agricultural crops, F. Crop. Res., 189, 68–74, https://doi.org/10.1016/j.fcr.2016.02.013, 2016.

FAO: Crops and climate change impact briefs. Climate-smart agriculture for more sustainable, resilient, and equitable food 795 systems, Rome, 202 pp., https://doi.org/10.4060/cb8030en, 2022.

FDRE: Ethiopia's Climate Resilient Green Economy: National Adaptation Plan, Addis Ababa, Ethiopia, 86 pp., 2019.

Fischer, G., Nachtergaele, F., Velthuizen, H. van, Chiozza, F., Franceschini, G., Hnery, M., Muchoney, D., and Tramberend, S.: Global agro-ecological zone V4 – Model documentation, https://doi.org/10.4060/cb4744en, 2021.

Foster, T. and Brozović, N.: Simulating Crop-Water Production Functions Using Crop Growth Models to Support Water Policy
800 Assessments, Ecol. Econ., 152, 9–21, https://doi.org/10.1016/j.ecolecon.2018.05.019, 2018.

Funk, C., Peterson, P., Landsfeld, M., Pedreros, D., Verdin, J., Shukla, S., Husak, G., Rowland, J., Harrison, L., Hoell, A., and Michaelsen, J.: The climate hazards infrared precipitation with stations - A new environmental record for monitoring extremes, Nat. Sci. Data, 2, https://doi.org/10.1038/sdata.2015.66, 2015.

Geerts, S. and Raes, D.: Deficit irrigation as an on-farm strategy to maximize crop water productivity in dry areas, Agric.
805 Water Manag., 96, 1275–1284, https://doi.org/10.1016/j.agwat.2009.04.009, 2009.

Grossi, A. and Dinku, T.: From research to practice: Adapting agriculture to climate today for tomorrow in Ethiopia, Front. Clim., https://doi.org/10.3389/fclim.2022.931514, 2022.

Global Yield Gap Atlas: www.yieldgap.org , last access: 13 August 2024.

Hadgu, G., Tesfaye, K., and Mamo, G.: Analysis of climate change in Northern Ethiopia: implications for agricultural
810 production, Theor. Appl. Climatol., 121, 733–747, https://doi.org/10.1007/s00704-014-1261-5, 2015.

Hamby, D. .: A review of techniques for parameter sensitivity analysis of environmental models, Environ. Monit. Assess., 32, 135–154, https://doi.org/10.1007/BF00547132, 1994.

Hartmann, M. and Six, J.: Soil structure and microbiome functions in agroecosystems, Nat. Rev. Earth Environ., 4, 4–18, https://doi.org/10.1038/s43017-022-00366-w, 2023.

815 Hatfield, J. L. and Dold, C.: Water-use efficiency: Advances and challenges in a changing climate, Front. Plant Sci., 10, 1–14, https://doi.org/10.3389/fpls.2019.00103, 2019.

Hawkins, R. H., Moglen, G. E., Ward, T. J., and Woodward, D. E.: Watershed Management 2020 99, in: Watershed Management 2020, 301–340, 2020.

He, J., Ma, B., and Tian, J.: Water production function and optimal irrigation schedule for rice (Oryza sativa L.) cultivation
820 with drip irrigation under plastic film-mulched, Sci. Rep., 12, 1–12, https://doi.org/10.1038/s41598-022-20652-3, 2022.

Holzworth, D. P., Huth, N. I., deVoil, P. G., Zurcher, E. J., Herrmann, N. I., McLean, G., Chenu, K., van Oosterom, E. J., Snow, V., Murphy, C., Moore, A. D., Brown, H., Whish, J. P. M., Verrall, S., Fainges, J., Bell, L. W., Peake, A. S., Poulton, P. L., Hochman, Z., Thorburn, P. J., Gaydon, D. S., Dalgliesh, N. P., Rodriguez, D., Cox, H., Chapman, S., Doherty, A., Teixeira, E., Sharp, J., Cichota, R., Vogeler, I., Li, F. Y., Wang, E., Hammer, G. L., Robertson, M. J., Dimes, J. P., Whitbread,

825   A. M., Hunt, J., van Rees, H., McClelland, T., Carberry, P. S., Hargreaves, J. N. G., MacLeod, N., McDonald, C., Harsdorf, J., Wedgwood, S., and Keating, B. A.: APSIM - Evolution towards a new generation of agricultural systems simulation, Environ. Model. Softw., 62, 327–350, https://doi.org/10.1016/j.envsoft.2014.07.009, 2014.

Hoogeveen, J., Faurès, J. M., Peiser, L., Burke, J., and Van De Giesen, N.: GlobWat - A global water balance model to assess water use in irrigated agriculture, Hydrol. Earth Syst. Sci., 19, 3829–3844, https://doi.org/10.5194/hess-19-3829-2015, 2015.

830   Hsiao, T. C., Heng, L., Steduto, P., Rojas-Lara, B., Raes, D., and Fereres, E.: Aquacrop-The FAO crop model to simulate yield response to water: III. Parameterization and testing for maize, Agron. J., 101, 448–459, https://doi.org/10.2134/agronj2008.0218s, 2009.

Hurni, H.: Soil and Water Conservation in Ethiopia: Guidlines for Development Agents, Bern Open Publishing (BOP), 117–123 pp., https://doi.org/10.7892/boris.80013, 2016.

835   IFPRI and CSA: Atlas of the Ethiopian Rural Economy, International Food Policy Research Institute, Washinton DC, https://doi.org/10.2499/0896291545, 2006.

van Ittersum, M. K., Cassman, K. G., Grassini, P., Wolf, J., Tittonell, P., and Hochman, Z.: Yield gap analysis with local to global relevance-A review, F. Crop. Res., 143, 4–17, https://doi.org/10.1016/j.fcr.2012.09.009, 2013.

Jägermeyr, J., Müller, C., Ruane, A. C., Elliott, J., Balkovic, J., Castillo, O., Faye, B., Foster, I., Folberth, C., Franke, J. A.,
840   Fuchs, K., Guarin, J. R., Heinke, J., Hoogenboom, G., Iizumi, T., Jain, A. K., Kelly, D., Khabarov, N., Lange, S., Lin, T. S., Liu, W., Mialyk, O., Minoli, S., Moyer, E. J., Okada, M., Phillips, M., Porter, C., Rabin, S. S., Scheer, C., Schneider, J. M., Schyns, J. F., Skalsky, R., Smerald, A., Stella, T., Stephens, H., Webber, H., Zabel, F., and Rosenzweig, C.: Climate impacts on global agriculture emerge earlier in new generation of climate and crop models, Nat. Food, 2, 873–885, https://doi.org/10.1038/s43016-021-00400-y, 2021.

845   Jimma, T. B., Demissie, T., Diro, G. T., Ture, K., Terefe, T., and Solomon, D.: Spatiotemporal variability of soil moisture over Ethiopia and its teleconnections with remote and local drivers, Theor. Appl. Climatol., 151, 1911–1929, https://doi.org/10.1007/s00704-022-04335-7, 2023.

Jones, J. W., Hoogenboom, G., Porter, C. H., Boote, K. J., Batchelor, W. D., Hunt, L. A., Wilkens, P. W., Singh, U., Gijsman, A. J., and Ritchie, J. T.: The DSSAT cropping system model, 235–265 pp., https://doi.org/10.1016/S1161-0301(02)00107-7,
850   2003.

Kang, Y., Khan, S., and Ma, X.: Climate change impacts on crop yield, crop water productivity and food security - A review, Prog. Nat. Sci., 19, 1665–1674, https://doi.org/10.1016/j.pnsc.2009.08.001, 2009.

Kassawmar, T., Zeleke, G., Bantider, A., Gessesse, G. D., and Abraha, L.: A synoptic land change assessment of Ethiopia's Rainfed Agricultural Area for evidence-based agricultural ecosystem management, Heliyon, 4, e00914,

855   https://doi.org/10.1016/j.heliyon.2018.e00914, 2018.

Kassawmar, T., Zeleke, G., Bantider, A., Gessesse, G. D., Abebe, S., Abraha, L., and Tadesse, M.: State of cropland availability in rainfed farming systems in Ethiopia: Alternative pathways to address landlessness and food insecurity. In: Ethiopia: Social and Political Issues, in: Ethiopia: Social and Political Issues, vol. 1, NOVA, 228–260, 2019.

Kassaye, A. Y., Shao, G., Wang, X., Shifaw, E., and Wu, S.: Impact of climate change on the staple food crops yield in
860   Ethiopia: implications for food security, Theor. Appl. Climatol., 145, 327–343, https://doi.org/10.1007/s00704-021-03635-8, 2021.

Kassie, B. T., Rötter, R. P., Hengsdijk, H., Asseng, S., Van Ittersum, M. K., Kahiluoto, H., and Van Keulen, H.: Climate variability and change in the Central Rift Valley of Ethiopia: Challenges for rainfed crop production, J. Agric. Sci., 152, 58–74, https://doi.org/10.1017/S0021859612000986, 2014.

865   Kukal, M. S. and Irmak, S.: Climate-Driven Crop Yield and Yield Variability and Climate Change Impacts on the U.S. Great Plains Agricultural Production, Nat. Sci. Rep., 8, 1–18, https://doi.org/10.1038/s41598-018-21848-2, 2018.

Kummu, M., Heino, M., Taka, M., Varis, O., and Viviroli, D.: Climate change risks pushing one-third of global food production outside the safe climatic space, One Earth, 4, 720–729, https://doi.org/10.1016/j.oneear.2021.04.017, 2021.

Laderach, P., Ramirez-Villegas, J., Prager, S. D., Osorio, D., Krendelsberger, A., Zougmore, R. B., Charbonneau, B., Van
870   Dijk, H., Madurga-Lopez, I., and Pacillo, G.: The importance of food systems in a climate crisis for peace and security in the Sahel, Int. Rev. Red Cross, 103, 995–1028, https://doi.org/10.1017/S1816383122000170, 2021.

Lala, J., Yang, M., Wang, G., and Block, P.: Utilizing rainy season onset predictions to enhance maize yields in Ethiopia, Environ. Res. Lett., 16, https://doi.org/10.1088/1748-9326/abf9c9, 2021.

Li, K., Pan, J., Xiong, W., Xie, W., and Ali, T.: The impact of 1.5 °C and 2.0 °C global warming on global maize production
875   and trade, Sci. Rep., 12, https://doi.org/10.1038/s41598-022-22228-7, 2022.

Liu, M., Wang, D., Chen, X., Chen, Y., Gao, L., and Deng, H.: Impacts of climate variability and land use on the blue and green water resources in a subtropical basin of China, Sci. Rep., 12, 1–11, https://doi.org/10.1038/s41598-022-21880-3, 2022a.

Liu, X., Liu, W., Tang, Q., Liu, B., Wada, Y., and Yang, H.: Global Agricultural Water Scarcity Assessment Incorporating Blue and Green Water Availability Under Future Climate Change, Earth's Futur., 10, https://doi.org/10.1029/2021EF002567,
880   2022b.

Lobell, D. B., Cassman, K. G., and Field, C. B.: Crop yield gaps: Their importance, magnitudes, and causes, Annu. Rev. Environ. Resour., 34, 179–204, https://doi.org/10.1146/annurev.environ.041008.093740, 2009.

Lobell, D. B., Schlenker, W., and Costa-Roberts, J.: Climate Trends and Global crop production since 1980 1980, 333, 1186–1189, https://doi.org/10.1126/science.1206376, 2011a.

885   Lobell, D. B., Bänziger, M., Magorokosho, C., and Vivek, B.: Nonlinear heat effects on African maize as evidenced by historical yield trials, Nat. Clim. Chang., 1, https://doi.org/10.1038/nclimate1043, 2011b.

Makurira, H., Savenije, H. H. G., Uhlenbrook, S., Rockström, J., and Senzanje, A.: Investigating the water balance of on-farm techniques for improved crop productivity in rainfed systems: A case study of Makanya catchment, Tanzania, Phys. Chem. Earth, 34, 93–98, https://doi.org/10.1016/j.pce.2008.04.003, 2009.

890   Manik, S. M. N., Pengilley, G., Dean, G., Field, B., Shabala, S., and Zhou, M.: Soil and crop management practices to minimize the impact of waterlogging on crop productivity, Front. Plant Sci., 10, 1–23, https://doi.org/10.3389/fpls.2019.00140, 2019.

Markos, D., Worku, W., and Mamo, G.: Exploring adaptation responses of maize to climate change scenarios in southern central Rift Valley of Ethiopia, Sci. Rep., 13, 1–18, https://doi.org/10.1038/s41598-023-39795-y, 2023.

Meinshausen, M., Nicholls, Z. R. J., Lewis, J., Gidden, M. J., Vogel, E., Freund, M., Beyerle, U., Gessner, C., Nauels, A.,
895   Bauer, N., Canadell, J. G., Daniel, J. S., John, A., Krummel, P. B., Luderer, G., Meinshausen, N., Montzka, S. A., Rayner, P. J., Reimann, S., Smith, S. J., Van Den Berg, M., Velders, G. J. M., Vollmer, M. K., and Wang, R. H. J.: The shared socio-economic pathway (SSP) greenhouse gas concentrations and their extensions to 2500, Geosci. Model Dev., 13, 3571–3605, https://doi.org/10.5194/gmd-13-3571-2020, 2020.

Mekonnen, M. M. and Hoekstra, A. Y.: The green, blue and grey water footprint of crops and derived crop products, Hydrol.
900   Earth Syst. Sci., 15, 1577–1600, https://doi.org/10.5194/hess-15-1577-2011, 2011.

Meng, M., Pu, X., Li, S., Zhang, Y., Wang, J., Xu, H., Hu, Y., Wang, J., and Wang, Y.: Sensitivities of rainfed maize production to root zone soil water , air temperature and shortwave radiation in the Sanjiang Plain under sub- humid cool-temperate climates, Water-Energy Nexus, 6, 131–136, https://doi.org/10.1016/j.wen.2023.09.003, 2023.

Moges, D. M. and Gangadhara, B. H.: Climate change and its implications for rainfed agriculture in Ethiopia, J. Water Clim.
905   Chang., 12, 1229–1244, https://doi.org/10.2166/wcc.2020.058, 2021.

Mohammadi, S., Rydgren, K., Bakkestuen, V., and Gillespie, M. A. K.: Impacts of recent climate change on crop yield can depend on local conditions in climatically diverse regions of Norway, Sci. Rep., 13, 1–12, https://doi.org/10.1038/s41598-023-30813-7, 2023.

Molden, D., Vithanage, M., de Fraiture, C., Faures, J. M., Gordon, L., Molle, F., and Peden, D.: Water Availability and Its Use
910   in Agriculture, Treatise Water Sci., 4, 707–732, https://doi.org/10.1016/B978-0-444-53199-5.00108-1, 2011.

Mthandi, J., Kahimba, F. C., Tarimo, A. K. P. R., Salim, B. A., and Lowole, M. W.: Root zone soil moisture redistribution in maize (<i>Zea mays</i> L.) under different water application regimes, Agric. Sci., 04, 521–528, https://doi.org/10.4236/as.2013.410070, 2013.

Mu, Q., Zhao, M., and Running, S. W.: MODIS Global Terrestrial Evapotranspiration (ET) Product (NASA MOD16A2/A3)

915   Algorithm Theoretical Basis Document Collection 5, 2019.

Müller, C., Cramer, W., Hare, W. L., and Lotze-Campen, H.: Climate change risks for African agriculture, Proc. Natl. Acad. Sci. U. S. A., 108, 4313–4315, https://doi.org/10.1073/pnas.1015078108, 2011.

Muluneh, A.: Impact of climate change on soil water balance, maize production, and potential adaptation measures in the Rift Valley drylands of Ethiopia, J. Arid Environ., 179, 104195, https://doi.org/10.1016/j.jaridenv.2020.104195, 2020.

920   Muñoz-Sabater, J., Dutra, E., Agustí-Panareda, A., Albergel, C., Arduini, G., Balsamo, G., Boussetta, S., Choulga, M., Harrigan, S., Hersbach, H., Martens, B., Miralles, D. G., Piles, M. M., Rodríguez-Fernández, N. J., Zsoter, E., Buontempo, C., and Thépaut, J.-N. N.: ERA5-Land: A state-of-the-art global reanalysis dataset for land applications, Earth Syst. Sci. Data, 13, 4349–4383, https://doi.org/10.5194/essd-13-4349-2021, 2021.

Nyakudya, I. W., Stroosnijder, L., and Nyagumbo, I.: Infiltration and planting pits for improved water management and maize 925   yield in semi-arid Zimbabwe, Agric. Water Manag., 141, 30–46, https://doi.org/10.1016/j.agwat.2014.04.010, 2014.

O'Neill, B. C., Tebaldi, C., Van Vuuren, D. P., Eyring, V., Friedlingstein, P., Hurtt, G., Knutti, R., Kriegler, E., Lamarque, J. F., Lowe, J., Meehl, G. A., Moss, R., Riahi, K., and Sanderson, B. M.: The Scenario Model Intercomparison Project (ScenarioMIP) for CMIP6, Geosci. Model Dev., 9, 3461–3482, https://doi.org/10.5194/gmd-9-3461-2016, 2016.

Park, S., Chun, J. A., Kim, D., and Sitthikone, M.: Climate risk management for the rainfed rice yield in Lao PDR using APCC 930   MME seasonal forecasts, Agric. Water Manag., 274, 107976, https://doi.org/10.1016/j.agwat.2022.107976, 2022.

Peleg, N., Molnar, P., Burlando, P., and Fatichi, S.: Exploring stochastic climate uncertainty in space and time using a gridded hourly weather generator, J. Hydrol., 571, 627–641, https://doi.org/10.1016/j.jhydrol.2019.02.010, 2019.

Pittelkow, C. M., Linquist, B. A., Lundy, M. E., Liang, X., van Groenigen, K. J., Lee, J., van Gestel, N., Six, J., Venterea, R. T., and van Kessel, C.: When does no-till yield more? A global meta-analysis, F. Crop. Res., 183, 156–168, 935   https://doi.org/10.1016/j.fcr.2015.07.020, 2015.

Poggio, L., De Sousa, L. M., Batjes, N. H., Heuvelink, G. B. M., Kempen, B., Ribeiro, E., and Rossiter, D.: SoilGrids 2.0: Producing soil information for the globe with quantified spatial uncertainty, Soil, 7, 217–240, https://doi.org/10.5194/soil-7-217-2021, 2021.

Qi, J., Lee, S., Zhang, X., Yang, Q., McCarty, G. W., and Moglen, G. E.: Effects of surface runoff and infiltration partition 940   methods on hydrological modeling: A comparison of four schemes in two watersheds in the Northeastern US, J. Hydrol., 581, 124415, https://doi.org/10.1016/j.jhydrol.2019.124415, 2020.

Raes, D., Steduto, P., Hsiao, T. C., and Fereres, E.: Aquacrop-The FAO crop model to simulate yield response to water: II. main algorithms and software description, Agron. J., 101, 438–447, https://doi.org/10.2134/agronj2008.0140s, 2009.

Raes, D., Steduto, P., Hsiao, T. C., and Fereres, E.: AquaCrop Version 7.1 Reference manual, Rome, 178 pp., 2022.

Ramirez-Villegas, J., Koehler, A. K., and Challinor, A. J.: Assessing uncertainty and complexity in regional-scale crop model simulations, Eur. J. Agron., 88, 84–95, https://doi.org/10.1016/j.eja.2015.11.021, 2017.

Rettie, F. M., Gayler, S., Weber, T. K. D., Tesfaye, K., and Streck, T.: Climate change impact on wheat and maize growth in Ethiopia: A multi-model uncertainty analysis, PLoS One, 17, 1–26, https://doi.org/10.1371/journal.pone.0262951, 2022.

Rezaei, E. E., Webber, H., Asseng, S., Boote, K., Durand, J. L., Ewert, F., Martre, P., and MacCarthy, D. S.: Climate change impacts on crop yields, Nat. Rev. Earth Environ., 4, 16, https://doi.org/10.1038/s43017-023-00491-0, 2023.

Richards, L. A.: Capillary conduction of liquids through porous mediums, J. Appl. Phys., 1, 318–333, https://doi.org/10.1063/1.1745010, 1931.

Ringersma, J., Batjes, N., and Dent, D.: Green Water: definitions and data for assessment, ISRIC – World Soil Information, 83 pp., 2003.

Rockström, J.: On-farm green water estimates as a tool for increased food production in water scarce regions, Phys. Chem. Earth, Part B Hydrol. Ocean. Atmos., 24, 375–383, https://doi.org/10.1016/S1464-1909(99)00016-7, 1999.

Rockström, J.: Water for food and nature in drought-prone tropics: Vapour shift in rain-fed agriculture, Philos. Trans. R. Soc. B Biol. Sci., 358, 1997–2009, https://doi.org/10.1098/rstb.2003.1400, 2003.

Rockström, J. and Gordon, L.: Assessment of Green Water Flows to Sustain Major Biomes of the World: Implications for Future Ecohydrological Landscape Management, Phys. Chem. Earth, Part B Hydrol. Ocean. Atmos., 26, 843–851, https://doi.org/10.1016/S1464-1909(01)00096-X, 2001.

Rockström, J., Karlberg, L., Wani, S. P., Barron, J., Hatibu, N., Oweis, T., Bruggeman, A., Farahani, J., and Qiang, Z.: Managing water in rainfed agriculture-The need for a paradigm shift, Agric. Water Manag., 97, 543–550, https://doi.org/10.1016/j.agwat.2009.09.009, 2010.

Rodell, M., Houser, P. R., Jambor, U. ., Gottschalck, J., Mitchell, K. ., Meng, C.-J., Arsenault, K., Cosgrove, B., Radakovich, J., Bosilovich, M., Entin, J. K. ., Walker, J. P., Lohmann, D. ., and Toll, D. .: THE GLOBAL LAND DATA ASSIMILATION SYSTEM, 2004.

Rosenzweig, C., Elliott, J., Deryng, D., Ruane, A. C., Müller, C., Arneth, A., Boote, K. J., Folberth, C., Glotter, M., Khabarov, N., Neumann, K., Piontek, F., Pugh, T. A. M., Schmid, E., Stehfest, E., Yang, H., and Jones, J. W.: Assessing agricultural risks of climate change in the 21st century in a global gridded crop model intercomparison, Proc. Natl. Acad. Sci. U. S. A., 111, 3268–3273, https://doi.org/10.1073/pnas.1222463110, 2014.

Ross, C. W., Prihodko, L., Anchang, J., Kumar, S., Ji, W., and Hanan, N. P.: HYSOGs250m, global gridded hydrologic soil groups for curve-number-based runoff modeling, Sci. data, 5, 180091, https://doi.org/10.1038/sdata.2018.91, 2018.

Rui, H. L. and Beaudoing, H.: README Document for NASA GLDAS Version 2 Data Products,

975 https://hydro1.gesdisc.eosdis.nasa.gov/data/GLDAS/README_GLDAS2.pdf, 2020.

Sapino, F., Pérez-Blanco, C. D., Gutiérrez-Martín, C., García-Prats, A., and Pulido-Velazquez, M.: Influence of crop-water production functions on the expected performance of water pricing policies in irrigated agriculture, Agric. Water Manag., 259, https://doi.org/10.1016/j.agwat.2021.107248, 2022.

Saxton, K. E. and Rawls, W. J.: Soil Water Characteristic Estimates by Texture and Organic Matter for Hydrologic Solutions,
980 Soil Sci. Soc. Am. J., 70, 1569–1578, https://doi.org/10.2136/sssaj2005.0117, 2006.

Schlenker, W. and Lobell, D. B.: Robust negative impacts of climate change on African agriculture, Environ. Res. Lett., 5, https://doi.org/10.1088/1748-9326/5/1/014010, 2010.

Schuol, J., Abbaspour, K. C., Yang, H., Srinivasan, R., and Zehnder, A. J. B.: Modeling blue and green water availability in Africa, Water Resour. Res., 44, 1–18, https://doi.org/10.1029/2007WR006609, 2008.

985 Schwartz, R. C., Domínguez, A., Pardo, J. J., Colaizzi, P. D., Baumhardt, R. L., and Bell, J. M.: A crop coefficient –based water use model with non-uniform root distribution, Agric. Water Manag., 228, 105892, https://doi.org/10.1016/j.agwat.2019.105892, 2020.

Segele, Z. T. and Lamb, P. J.: Characterization and variability of Kiremt rainy season over Ethiopia, Meteorol. Atmos. Phys., 89, 153–180, https://doi.org/10.1007/s00703-005-0127-x, 2005.

990 Senay, G. B., Kagone, S., and Velpuri, N. M.: Operational Global Actual Evapotranspiration :, 2020.

Serur, A. B.: Modeling blue and green water resources availability at the basin and sub-basin level under changing climate in the Weyb River basin in Ethiopia, Sci. African, 7, e00299, https://doi.org/10.1016/j.sciaf.2020.e00299, 2020.

Setegn, S. G., Rayner, D., Melesse, A. M., Dargahi, B., Srinivasan, R., and Wörman, A.: Climate Change Impact on Agricultural Water Resources Variability in the Northern Highlands of Ethiopia, in: Nile River basin climate, hydrology and
995 water use, edited by: Melesse, A. M., 2011.

Siad, S. M., Iacobellis, V., Zdruli, P., Gioia, A., Stavi, I., and Hoogenboom, G.: A review of coupled hydrologic and crop growth models, Agric. Water Manag., 224, 105746, https://doi.org/10.1016/j.agwat.2019.105746, 2019.

Sishu, F. K., Tilahun, S. A., Schmitter, P., and Steenhuis, T. S.: Revisiting the Thornthwaite Mather procedure for baseflow and groundwater storage predictions in sloping and mountainous regions, J. Hydrol. X, 24, 100179,
1000 https://doi.org/10.1016/j.hydroa.2024.100179, 2024.

Smedema, L. K. and Rycroft, D. W.: Land drainage: planning and design of agricultural drainage systems., 0, 183–184, https://doi.org/10.1016/0378-3774(85)90006-x, 1983.

Smilovic, M., Gleeson, T., and Adamowski, J.: Crop kites: Determining crop-water production functions using crop

coefficients and sensitivity indices, Adv. Water Resour., 97, 193–204, https://doi.org/10.1016/j.advwatres.2016.09.010, 2016.

1005   Spinoni, J., Vogt, J., Naumann, G., Carrao, H., and Barbosa, P.: Towards identifying areas at climatological risk of desertification using the Köppen-Geiger classification and FAO aridity index, Int. J. Climatol., 35, 2210–2222, https://doi.org/10.1002/joc.4124, 2015.

Sposito, G.: Green Water and Global Food Security, Vadose Zo. J., 12, 1–6, https://doi.org/10.2136/vzj2013.02.0041, 2013.

Steduto, P., Hsiao, T. C., Raes, D., and Fereres, E.: Aquacrop-the FAO crop model to simulate yield response to water: I.
1010   concepts and underlying principles, Agron. J., 101, 426–437, https://doi.org/10.2134/agronj2008.0139s, 2009.

Steduto, P., Hsiao, T. C., Fereres, E., and Raes, D.: Crop yield response to water, 505 pp., 2012.

Stöckle, C. O., Donatelli, M., and Nelson, R.: CropSyst, a cropping systems simulation model, Eur. J. Agron., 18, 289–307, https://doi.org/10.1016/S1161-0301(02)00109-0, 2003.

Teferi, E., O'Donnell, G., Kassawmar, T., Mersha, B. D., and Ayele, G. T.: Enhanced Soil Moisture Retrieval through
1015   Integrating Satellite Data with Pedotransfer Functions in a Complex Landscape of Ethiopia, Water (Switzerland), 15, https://doi.org/10.3390/w15193396, 2023.

Teng, B. and Parinussa, R.: README Document for NASA GLDAS Version 2 Data Products. Goddard Earth Sciences Data and Information Services Center (GES DISC). NASA, 32, 2021.

Tenreiro, T. R., García-Vila, M., Gómez, J. A., Jimenez-Berni, J. A., and Fereres, E.: Water modelling approaches and
1020   opportunities to simulate spatial water variations at crop field level, Agric. Water Manag., 240, 106254, https://doi.org/10.1016/j.agwat.2020.106254, 2020.

Teutschbein, C. and Seibert, J.: Bias correction of regional climate model simulations for hydrological climate-change impact studies: Review and evaluation of different methods, J. Hydrol., 456–457, 12–29, https://doi.org/10.1016/j.jhydrol.2012.05.052, 2012.

1025   Tittonell, P. and Giller, K. E.: When yield gaps are poverty traps: The paradigm of ecological intensification in African smallholder agriculture, F. Crop. Res., 143, 76–90, https://doi.org/10.1016/j.fcr.2012.10.007, 2013.

UNFCCC: Progress in the Formulation and Implementation of Naps, 2021.

USDA: Urban Hydrology for Small Watersheds, 164 pp., 1985.

Wakjira, M. T.: Understanding the impacts of climate variability and change on rainfed crop production in Ethiopia, ETH
1030   Zurich, 244 pp., https://doi.org/10.3929/ethz-b-000672129, 2024.

Wakjira, M. T., Peleg, N., Anghileri, D., Molnar, D., Alamirew, T., Six, J., and Molnar, P.: Rainfall seasonality and timing: implications for cereal crop production in Ethiopia, Agric. For. Meteorol., 310, 108633,

https://doi.org/10.1016/J.AGRFORMET.2021.108633, 2021.

Wakjira, M. T., Peleg, N., Molnar, P., and Burlando, P.: Bias-corrected and downscaled ERA5-Land 2-m air temperature dataset for Ethiopia for the period 1981-2010, https://doi.org/10.3929/ethz-b-000546574, 2022.

Wakjira, M. T., Peleg, N., Burlando, P., and Molnar, P.: Gridded daily 2-m air temperature dataset for Ethiopia derived by debiasing and downscaling ERA5-Land for the period 1981–2010, Data Br., 46, 108844, https://doi.org/10.1016/j.dib.2022.108844, 2023.

Warren, R. F., Wilby, R. L., Brown, K., Watkiss, P., Betts, R. A., Murphy, J. M., and Lowe, J. A.: Advancing national climate change risk assessment to deliver national adaptation plans, Philos. Trans. R. Soc. A Math. Phys. Eng. Sci., 376, https://doi.org/10.1098/rsta.2017.0295, 2018.

Williams, J. .: The erosion-productivity impact calculator (EPIC) model: a case history, Philos. Trans. R. Soc. London. Ser. B Biol. Sci., 329, 421–428, https://doi.org/10.1098/rstb.1990.0184, 1990.

Yang, M., Wang, G., Sun, Y., You, L., and Anyah, R.: Water stress dominates the projected maize yield changes in Ethiopia, Glob. Planet. Change, 228, https://doi.org/10.1016/j.gloplacha.2023.104216, 2023.

Zhang, Q., Yuan, Q., Jin, T., Song, M., and Sun, F.: SGD-SM 2.0: an improved seamless global daily soil moisture long-term dataset from 2002 to 2022, Earth Syst. Sci. Data, 14, 4473–4488, https://doi.org/10.5194/essd-14-4473-2022, 2022.

Zhang, Y., Kong, D., Gan, R., Chiew, F. H. S., McVicar, T. R., Zhang, Q., and Yang, Y.: Coupled estimation of 500 m and 8-day resolution global evapotranspiration and gross primary production in 2002–2017, Remote Sens. Environ., 222, 165–182, https://doi.org/10.1016/j.rse.2018.12.031, 2019.